LAWRENCE
LIVERMORE
NATIONAL
LABORATORY

UCRL-JRNL-233955

Measurements of the intercombination and forbidden lines from helium-like ions in Tokamaks and Electron Beam Ion Traps

M. Bitter, K. W. Hill, S. von Goeler, W. Stodiek, P. Beiersdorfer, J. E. Rice, A. Ince-Cushman

August 24, 2007

Canadian Journal of Physics

Measurements of the intercombination and forbidden lines from helium-like ions in Tokamaks and Electron Beam Ion Traps

[PACS: 52.55.Fa (Tokamaks); 32.30.Rj (X-ray spectra)]

M. Bitter*, K. W. Hill, S. von Goeler, W. Stodiek

Princeton Plasma Physics Laboratory,
P. O. Box 451, Princeton, New Jersey 08543, USA

P. Beiersdorfer

Lawrence Livermore National Laboratory
7000 East Avenue-Livermore, California 94550, USA

J. E. Rice, A. Ince-Cushman

Plasma Science and Fusion Center, MIT
77 Massachusetts Avenue, Cambridge, Massachusetts 902139, USA

***email:** **bitter@pppl.gov**

phone: **(USA)-609-243-2582**

fax: **(USA)-609-243-2665**

ABSTRACT

The paper reviews the results from tokamak experiments for the line ratios x/w, y/w, and z/w from helium-like ions with Z in the range from 14 to 28. With exception of the DITE experiments, where these line ratios were found to be in agreement with theoretical predictions, all other tokamak experiments yielded values that were significantly larger than predicted. The reasons for these discrepancies are not yet understood. It is possible that radial profile effects were not properly taken into account in the majority of the tokamak experiments. The paper also gives a short historical review of the X-ray diagnostic developments and also presents very recent data from a new type of X-ray imaging crystal spectrometer, which records spatially resolved spectra with a spatial resolution of about 1 cm in the plasma. These new data can be Abel inverted, so that it will be possible to determine line ratios at each radial position in the plasma. Effects of radial profiles, which may have affected the chord-integrated measurements of the past, will thus be eliminated in the future.

L. Introduction

The main diagnostic applications of the X-ray spectroscopy of tokamak plasmas, which has by now been pursued for about three decades, are measurements of the ion temperature and plasma rotation velocity from the Doppler width and Doppler shift of X-ray lines with high-resolution crystal spectrometers. These measurements are usually performed with use of the line radiation of helium-like ions from elements with atomic number Z in the range from 18 to 36, which are either present in the plasma as intrinsic impurities or added in small amounts for diagnostic purposes. The spectra of helium-like ions are preferred for diagnostic applications because this ion charge state can exist in the plasma over a wide range of electron temperatures. Tokamak experiments have thus accumulated a wealth of data on the spectra from helium-like ions over the last 30 years.

Very important for the interpretation of these spectra was the collaboration with atomic physicists, who provided theoretical data on wavelengths and excitation processes and who performed necessary, additional, experimental studies on electron beam ion traps. Such collaborations will be even more needed for the experiments on ITER, where plasmas with central electron and central ion temperatures above 10 keV must be diagnosed. A foretaste of what is to be expected from ITER was obtained from the high-power heating plasma experiments on JET and TFTR, where plasmas with ion temperatures of >20 keV were produced by intense auxiliary neutral-beam and RF heating. Under these conditions, the Doppler broadening was so large that the spectral features were blended with each other and that reliable measurements of the ion and

electron temperature from the observed spectral data could only be made by least-squares fit comparisons with synthetic spectra, which were constructed from theoretical predictions. Such theoretical predictions must include all the spectral features; and they must also be very accurate, with respect to both the wavelengths and the contributions from the relevant excitation processes.

With respect to the data from tokamak experiments on the spectra of helium-like ions, we can now say that the predictions for the numerous dielectronic satellites, which are associated with the helium-like resonance line, and the inner-shell excited lithium-and beryllium-like satellites are in excellent agreement with the experimental data, but that the ratios of the helium-like intercombination and the forbidden lines with respect to the resonance line are generally found to be larger than predicted. The reason for these discrepancies between theory and experiment, which were found in most tokamak measurements, are not yet understood; but they may have been caused by profile effects, which were not properly taken into account in the data analysis.

Fortunately, there are new instrumental developments underway, which will make it possible to record spectra from many sightlines through the plasma simultaneously with a spatial resolution of about 1 cm in the plasma. The spectral data obtained with these instruments can be Abel inverted, so that line widths, line shifts, and line ratios can be determined locally, at each point along a plasma radius, and profile effects, which may have affected the X-ray measurements on tokamak plasma in the past, can be eliminated. The progress in the diagnosis of tokamak plasmas, in particular, the diagnosis of the

plasmas on ITER and other large future devices, will therefore also depend on the development of new instrumentation.

This paper is organized as follows: Section II, is a historical review on the development of X-ray instrumentation for the X-ray diagnosis of tokamak plasmas. This brief review will illustrate how diagnostic challenges were overcome by new instrumentation and advances in atomic physics. Sections III, IV, and V are devoted to a review and discussion of the data on the helium-like line ratios from tokamaks and electron beam ion traps. Section VI will present the first spatially resolved spectra of helium-like ArXVII, which were recently obtained on Alcator C-Mod with a new type of X-ray imaging crystal spectrometer. This new spectrometer is also a prototype for the X-ray crystal spectrometers on ITER.

II. Historical Notes

The development of instrumentation for the X-ray diagnosis of tokamak plasmas was actively pursued since the early 1970's, soon after the experiments at the T3 tokamak at the Kurchatov Institute in Moscow had demonstrated that plasmas with core electron temperatures of 1 keV could be produced and confined for several ms [1]. Within a short time after the publication of these results the tokamak concept was worldwide accepted as the most promising experimental device in magnetic confinement nuclear fusion energy research, and soon even higher electron temperatures were achieved, so that the x-ray emission from tokamak plasmas became a more and more prominent feature, which was increasingly used for the diagnosis of the hot core of the plasma. Pioneers in the development of new instrumentation were W. Stodiek and S. von Goeler in Princeton,

who invented many of the X-ray diagnostic systems, which are now standard equipment for tokamak experiments. This development followed a very logical path and was driven by questions, which are still important today.

One of the first X-ray diagnostic systems was the X-ray pulse-height analysis system [2]. It was designed for measurements of the energy distribution of the X-ray emission from the ST tokamak with the primary goals to develop an independent diagnostic for the core electron temperature and to obtain information on runaway electrons, since there was a concern that the electron energy distribution in tokamak plasmas might not be thermal. This concern was also shared by W. Stodiek, who was skeptical with respect to the results from the T3 experiments. The spectra obtained with the pulse-height analysis system from the ST plasmas - see Fig. 1- were indeed revealing. They consisted of two distinctive parts: a 'thermal' continuum at photon energies < 10 keV with an exponential dependence on photon energy; and a high-energy tail at photon energies above 10 keV, which had to be attributed to the presence of runaway electrons. Superimposed on the thermal continuum were peaks, which were ascribed to the K- and L-shell line radiations from metal impurities. The values for the electron temperature, which were derived from the slope of the thermal continuum, were in good agreement with the results from laser scattering, so that, as intended, the pulse-height analysis system could be used as an alternative diagnostic to Thomson scattering for the core electron temperature. However, the detailed analysis of the X-ray spectra was complex due to the fact that the absolute intensity of the thermal continuum was by factors of 5 to 100 higher than what was expected for a pure hydrogen plasma, if one considered only the contributions from the

free-free hydrogenic bremsstrahlung and free-bound recombination radiation. These discrepancies between the observed and predicted continuum intensities and the presence of impurity lines in the observed spectra indicated that impurities played an essential role and that a full description of the observed radiation required knowledge of the impurity ion charge-state distributions and a distinction between the contributions from low-Z and high-Z elements. The presence of high-Z impurities complicated the analysis substantially, since one had to deal with ions from different elements and since the recombination radiation depends sensitively on the charge state of the ion, which in turn is determined by the rates of ionization and - dielectronic and radiative - recombination, and effects of finite confinement due to the fact that the transport of ions between hot and cold regions of the plasma leads to deviations from the local coronal equilibrium. The rate coefficients for the various processes were not well known at the time of the ST experiments, and there was also a debate about whether dielectronic recombination would be important in tokamak plasmas. Many thought of this process, which requires the resonant capture of an electron into an excited state of the recombining ion and a subsequent stabilizing radiative transition, as something 'esoteric'; and it was generally assumed that this process did not play a role in tokamak plasmas at all. It is, therefore, noteworthy, that the question about the importance of dielectronic recombination had already been raised much earlier, in a letter of 1961 by A. Unsöld to M. J. Seaton - see ref. [3]. In his letter, Unsöld said that his efforts to explain the ionization equilibrium of the solar corona had ended in a 'dilemma'. He wondered whether important processes of recombination had been overlooked, and he asked Seaton for a theoretical estimate of the contributions from dielectronic recombination. The article by Seaton and Storey (3) is a

thorough review of the theoretical work on dielectronic recombination during the period from 1939 until 1976 with a discussion of important contributions by Bates, Burgess, Bely, Bhalla, Dubau, Gabriel, and others. However, accurate predictions about the contributions from dielectronic recombination to the ionization equilibrium and X-ray spectra from tokamak plasmas were only emerging at the time of the ST experiments.

To address the questions, which were raised by the pulse-height analysis data, it was necessary to focus the attention on the line radiation from impurities and to design new, high-resolution instruments that were able to resolve the X-ray line spectra from different ion charge states. These requirements led to the development and use of X-ray crystal spectrometers for the diagnosis of tokamak plasmas. Results from first crude measurements of the Kα-line spectra of iron with a X-ray crystal spectrometer on ST were reported in ref. [4]. The experimental data were compared with synthetic spectra constructed from theoretical data by A. L. Merts and R. D. Cowan, which also included predictions about the contributions from dielectronic recombination to the spectra from different ion charge states – see Fig. 2. These data permitted only a qualitative comparison with the theoretical predictions due to the fact that they had been accumulated from several ST discharges with varying electron temperature. But even this qualitative comparison showed that the contributions from dielectronic recombination were significant. After these preliminary results, the iron line radiation was more thoroughly investigated on the PLT tokamak with a much improved X-ray curved crystal spectrometer with the stated goal ‘to experimentally verify the validity and accuracy of theoretical predictions based on coronal equilibrium and test their applicability to

tokamak plasmas' [5]. The new spectrometer consisted of a cylindrically bent 6x1.5 $in.^2$ 220-germanium crystal with a radius of curvature of 2.42 m and a position-sensitive multi-wire proportional counter in the Johann configuration [6] – see Fig. 3. The Johann configuration made it possible to observe the features from all the ion charge states simultaneously, since the instrument covered a sufficiently large spectral range. This was a significant improvement with regard to the situation on ST, where a flat crystal spectrometer had been used and where the positions of crystal and detector had to be adjusted between plasma discharges to access to a different wavelength range. The new instrument had a spectral resolution of 4 eV at 6400 eV, which was more than sufficient to resolve the radiation from different iron charge states, since the energy of the *1s-2p* transition increases by about 40 eV for each L-shell electron removed between charge states from Fe^{17+} to Fe^{24+}. Moreover, due to the fact that it was equipped with a multi-wire proportional counter, it was possible to obtain time-resolved spectra from a single tokamak discharge. Spectra from several hundred PLT discharges with central electron temperatures in the range from 800 to 1500 eV were analyzed by comparing the data with the theoretical predictions by Merts and Cowan – see Fig. 4. Based on this analysis it was concluded that coronal equilibrium was satisfied in the central region of the plasma, within a factor of 2 uncertainty, associated with the ionization cross sections used in the computations.

An entirely new challenge for the PLT experiments was the measurement of the ion temperature in the hot core of the plasma, since the plasma diameter on PLT was much larger than on ST. The standard techniques of the time for ion-temperature

measurements, the so-called 'passive' neutral-charge-exchange diagnostic and Doppler broadening measurements of the VUV line radiation, became problematic with increasing plasma diameter and electron temperature. The 'passive' neutral-charge-exchange diagnostic, which is based on a measurement of the energy distribution of hydrogen atoms escaping from the plasma, cannot be used for the diagnosis of the central ion temperature if the mean free path for neutral charge exchange is much smaller than the diameter of the plasma; and the VUV line radiation was primarily emitted from the edge of the plasma at higher central electron temperatures. On the other hand, as the electron temperatures increased, a larger fraction of the electromagnetic radiation was emitted in the X-ray region. It was, therefore, examined whether the central ion temperature could be determined from Doppler broadening measurements of X-ray lines. The experiments by Hill et al. [5] had shown that the *1s-2p* resonance line of helium-like iron (FeXXV) at 1.85 Å was a prominent spectral feature for central electron temperatures above 1.2 keV. Since this line was also well separated from other spectral features, it seemed to be appropriate for Doppler broadening measurements. In order to perform such measurements, the spectral resolution of the spectrometer was increased to $\lambda/\Delta\lambda = 15000$ by replacing the 220-germanium crystal with a 2243-quartz crystal, which had a radius of curvature of 3.33 m. As the proof-of-principle experiment on PLT were successful, the crystal spectrometer became an important diagnostic for the central ion temperature; and it provided crucial data on the central ion temperature during the first neutral-beam heating experiments on PLT, which produced plasmas with core ion temperatures of 4 keV [7].

It was a fortunate coincidence that, at the time of these PLT experiments, detailed theoretical calculations for the spectra of helium-like ions became also available. Gabriel [8] and Bahalla et al. [9] published data on the *n=2* transitions for the main helium-like lines and the associated dielectronic and inner-shell excited satellites for a number of ions, which are important for the study of solar flares, and Vainsthein and Safronova [10] published such data for helium- and hydrogen-like ions in the isoelectronic sequences from Z = 4 to Z=34. Even more elaborate calculations [11-13] for the satellite spectra of helium-like iron (FeXXV) were performed in preparation for the solar flares observations with the Solar Maximum Mission Satellite in 1980. These latter calculations yielded theoretical data for the dielectronic satellite transitions $1s2pnl\text{-}1s^2nl$ with $n=3-6$ and additional excitation processes for the helium-like lines, which included, besides direct electron impact excitation from the ground state, also the electron impact excitation to *higher-n* levels and the population of the *n=2* states by cascading, and the excitation by inner-shell ionization. Since a high-resolution crystal spectrometer for Doppler broadening measurements of the Fe XXV resonance line was already in place on PLT, it was only natural to use this instrument for an experimental verification of these new theoretical predictions. A dedicated experiment was performed in December 1978, where the satellite spectra of the FeXXV resonance line were recorded from a series of PLT discharges with different central electron temperatures. Figures 5 and 6 show the results, which were obtained from this experiment, and a table with explanations of the observed spectral features. Except for the helium-like line ratio, x/w, y/w, and z/w, which were higher than predicted, the observed spectra were found to be in excellent agreement with the theoretical predictions. Hence, the comparison between experimental data and

theoretical predictions thus demonstrated that the line ratios of the dielectronic and inner-shell excited satellites with respect to the helium-like resonance line could be used for the diagnosis of the central electron temperature and measurements of the ionization equilibrium [14].

X-ray crystal spectrometers are now standard diagnostic equipment in tokamak experiments, and a wealth of atomic data on the spectra of hydrogen-, helium-, and neon-like ions [15] has been obtained from tokamak plasmas over the last three decades. Reviews of the diagnostic systems and results from tokamak experiments are given in refs. [16-18].

We conclude this section with a brief description of the X-ray crystal spectrometers on JET and TFTR, since the technical problems that had to be overcome on these devices and the spectral data that were obtained from these high-power plasma heating experiments give a foretaste of what is to be expected from ITER. Since the Tokamak Fusion Test Reactor (TFTR) and Joint European Torus (JET) were designed for DT experiments and a demonstration of fusion breakeven, the plasma diagnostic systems had to operate in an environment of intense neutron and gamma radiation. The instrumentation for measurements of the ion temperature and plasma rotation on TFTR consisted of a massively shielded Johann type, X-ray crystal spectrometer in the TFTR Test Cell with a central line of sight in the horizontal mid-plane of TFTR [19] and an array of up to five Johann X-ray crystal spectrometers with near-vertical sightlines for profile-measurements of the ion temperature [20, 21]. The latter instruments were located

in the TFTR basement, which was shielded by a 1.83 m thick concrete ceiling, so that the background of neutron and gamma radiation in the basement was by three orders of magnitude smaller than in the TFTR Test Cell. Additional shielding of the detectors was provided by 20 cm thick walls of lead and borated polyethylene, which surrounded the detectors. The dimensions of these spectrometers were large as the radii of curvature of the cylindrically bent crystals varied between 10 and 12 m. A Johann spectrometer of even larger dimensions, using a quartz crystal with a radius of curvature of 25 m and a Bragg angle of 50.75°, was built for JET by the ENEA Laboratories in Frascati [22]. The layout of this instrument was such that the crystal and detector could be positioned outside the biological shield, a 3 m thick concrete wall separating the torus hall from the diagnostic hall. The sightline of this spectrometer passed through the horizontal mid-plane of JET and included an angle of 35° with a major radius of the torus at the magnetic axis, so that a large fraction of 57% of the central toroidal plasma rotation velocity could be observed as a Doppler shift. Because of its large dimensions, the dispersion and spectral resolution ($\lambda/\Delta\lambda = 20000$) of the instrument were very high, so that only a small spectral range, which included the resonance line of helium-like nickel at 1.59 Å and associated dielectronic satellites in the immediate neighborhood, could be observed.

The parameters of the JET and TFTR experiments - with plasma currents of $\geq$ 2 MA and auxiliary heating of up to 45 MW by neutral beam injection and up to 12 MW by radio-frequency, ion-cyclotron resonance heating, in addition to Ohmic heating - exceeded by far those of previous tokamak experiments. Hence, the ion and electron temperatures, which were in the range from 1-3 keV and 3-6 keV in plasmas with purely Ohmic

heating, reached values of 30 keV and 10 keV, respectively, in plasmas with intense auxiliary heating. For ion temperatures > 20 keV, Doppler broadening was so large that the spectral features were blended with each other and that the measurement of the ion temperature became complicated. Figures 7 - 9 show, as an example, the time history of the central ion temperature from a TFTR plasma with auxiliary neutral-beam heating of 20 MW from 3.0 to 4.0 s and the satellite spectra of the $1s^2 - 1s2p$ resonance line of FeXXV, which were recorded during the periods from 2.5 to 3.0 s and 3.5 to 4.0 s, respectively. The spectrum in Fig. 8, which was taken during the Ohmic heating phase, shows 10 well resolved features, whereas the spectrum in Fig. 9, which was taken during the phase of intense neutral beam heating, seems to consist of only four wide humps, so that, at first sight, an ion-temperature measurement appeared to be impossible. The information contained in this spectrum could only be brought out by a least-squares fit comparison of the experimental data with a synthetic spectrum constructed from detailed theoretical predictions for all the spectral components, considering the ion and electron temperatures, the position and intensity of the $1s^2$-$1s2p$ resonance line, and the relative abundance of the lithium-like and helium-like charge states, FeXXIV and FeXXV, as variable parameters [23]. The synthetic spectrum consisted of more than 150 spectral lines, which included the main helium-like lines, ***w***: $1s^2\ ^1S_0$ -$1s2p\ ^1P_1$, ***x***: $1s^2\ ^1S_0$ -$1s2p\ ^3P_2$, ***y***: $1s^2\ ^1S_0$ -$1s2p\ ^3P_1$, ***z***: $1s^2\ ^1S_0$-$1s2p\ ^3S_1$, and the dielectronic and inner-shell excited satellites $1s2pnl - 1s^2nl$ with $n=2$-6 [24]. The numerous dielectronic satellites with $n>3$ merge with the resonance line ***w***, so that they cannot be resolved even when the ion temperature is low, e.g. in the range of 1 – 2 keV. Since the intensity of dielectronic satellites decreases with n as n^{-3}, the contributions from satellites with $n>6$ should be

negligible. The results obtained from the least-squares fit of the spectra in Figs. 8 and 9 are shown in the table in Fig. 10. The fact that the least squares fit value for the electron temperature - obtained by comparing the predicted intensity ratios for the dielectronic satellites and the resonance line ***w*** with the experimental data - was in excellent agreement with the central electron temperature of the radial electron-temperature profile obtained from Thomson scattering measurements (see Fig. 11) provided convincing evidence that the synthetic spectrum included, indeed, all the essential features [23]; it also indicated that the FeXXV satellite spectra were predominantly emitted from the hot center of the plasma, so that the least-squares fit value for the ion temperature could also be considered to represent the central ion temperature. Further corroborating evidence for this conclusion was obtained from the fact that the ion-temperature result from the crystal spectrometer also agreed with central value of the ion temperature profile measured by the charge exchange spectroscopy [25]. - Although it should be mentioned that the analysis of the charge-exchange spectra from plasmas with powerful neutral beam injection was also not without intricacies, since the observed spectral line profile consisted of two Doppler shifted components, which originated from the center and edge of the plasma, and since the intensity of the component from the center of the plasma that was used for the measurement of the central ion temperature became relatively weak as the plasma density increased with the injected total neutral beam power. - We conclude from these experiments that detailed knowledge of all the spectral features and excitation processes will also be absolutely necessary for reliable measurements of the ion temperature on ITER.

III. Intercombination and Forbidden Lines

Gabriel and Jordan [26] first pointed out that the intensity ratios of the $1S_0 - 2\ ^3P_{1,2}$ intercombination lines *(x, y)*, the $1S_0 - 2\ ^3S_1$ forbidden line *(z)*, and the $1S_0 - 2\ ^1P_1$ resonance line *(w)* of helium-like ions should be density sensitive – and, therefore, usable as an electron density diagnostic - when the rates for a de-excitation by electron collisions are comparable to the radiative transition rates for the $n = 2$ triplet states. Since the radiative transition rates for these states vary strongly with the atomic number Z (see Table III), the latter condition is fulfilled in density regimes that are specific for each ion. Following McWhirter [28], we illustrate the density dependence of the helium-like line intensities in Fig. 12, using OVII as an example. We distinguish regimes of 'very high', 'high', 'intermediate', and 'low' density: At very high densities (not shown in Fig. 12), the electron collision rates exceed the fastest radiative transition rate, so that no line radiation can be observed, and all levels are populated according to the Saha-Boltzmann equation. In the high density regime the singlet levels (except the $2\ ^1S$) decay radiatively and the $^1S_0 - ^1P_1$ line can be observed, while the triplet levels are subject to collisional transfer to levels, which can radiate or which can be ionized. In the intermediate density regime the intercombination transition, $1\ ^1S_0 - 2\ ^3P_1$ (spectral line **y**), is the most probable decay route for the metastable level $2\ ^3S_1$, since the $2\ ^3P$ levels are rapidly populated from the $2\ ^3S_1$ level by collisions, which also ensure that the sublevels $2\ ^3P_0$, $2\ ^3P_1$, and $2\ ^3P_2$ are statistically populated. At somewhat lower densities, also the $1\ ^1S_0 - 2\ ^3P_2$ magnetic quadrupole transition (line **x**) contributes to this decay mechanism; in the case of OVII, the $2\ ^3P_1$ and $2\ ^3P_2$ levels are, however, so close that the lines **y** and **x** cannot be resolved. At still lower densities the metastable singlet level $2\ ^1S$ has a greater probability to decay

by two-photon emission than by collisions to the $^1P_1$ level, so that 1 ^1S – $^1P_1$ line becomes relatively weaker. Finally, at even lower densities the relativistic magnetic dipole transition 1 $^1S_0$ - 2 $^3S_1$ level (the forbidden line **z**) can be observed.

The collision rate coefficients, used to construct Fig. 12, were obtained by Bely [29] and Burgess [30], using the Coulomb-Born-Oppenheimer approximation. These early theoretical calculations suffer from large uncertainties and also neglect important mechanisms, such as the population of the higher *1snl* levels *(with n >2)* by collisions from the $1s^2\,^1S_0$ helium-like ground state - or by recombination of hydrogen-like ions - followed by cascading to the helium-like n = 2 levels, and the population of the *1s2s* helium-like state by inner-shell ionization of the lithium-like $1s^2 2s$ ground state. Figure 12 gives, therefore, only a qualitative picture of the density dependence of the helium-like lines. More complete and more accurate calculations of the excitation rate coefficients for the n = 2 levels of helium-like ions were performed by Keenan et al. [31], using the R-matrix code of Burke and Robb [32]. These later calculations also include effects of cascading.

The ratios, $R = \frac{z}{x+y}$ and $G = \frac{x+y+z}{w}$, are convenient expressions to describe the density and temperature sensitivity of the helium-like lines, and these expressions are, therefore, commonly used for the diagnosis of the electron density and electron temperature in stellar atmospheres and laser-produced plasmas. The R and G ratios are less important for the diagnosis of tokamak plasmas, where the electron density and electron temperature are usually determined by Thomson scattering and other

independent methods. Yet due to the fact that tokamak plasmas are well diagnosed and well reproducible, they represent an ideal environment for tests of theoretical predictions. Tokamak experiments are often also equipped with high-resolution X-ray crystal spectrometers for Doppler measurements of the ion temperature and plasma rotation velocity. These instruments provide spectral data with well-resolved spectral features. - In this section, we review the results from measurements of the intensity ratios of the helium-like lines w, x, y, and z in various tokamak experiments.

Keenan et al. investigated the spectra of helium-like Si XIII [33] and Mg XI [34] on the DITE tokamak and compared their experimental results for the R and G ratios with predictions derived from new R-matrix code calculations of the electron impact excitation rates for the helium-like lines [32] and [31]. Figures 13 and 14 show their results. The authors concluded that their experimental data are in good/excellent/ agreement with the theoretical predictions, since the discrepancies are typically 8% in R and 5% in G for SiXIII and 3% in R and 9% in G for MgXI. We note that these results from DITE are exceptional, since in all other tokamak experiments the ratios of the helium-like lines were found to be higher than predicted.

Kato et al [35] recorded time-resolved TiXXI-TiXIX line spectra from a plasma with Ohmic heating and neon puffing on JIPP-T-II-U tokamak with a high resolution crystal spectrometer and used a collisional radiative model, which included the cascade contributions from highly excited states as well as recombination processes, to analyze the observed spectra. The line ratios x/w and y/w were always found to be more than

twice as large as the theoretical predictions. However, the experimental data for z/w were in good agreement with calculations when the inner-shell ionization of Li/Like ions was included. Figure 15a shows an observed spectrum (dots) from an ohmically heated plasma with neon puffing and a calculated synthetic spectrum (solid lines), where the hatched area represents the contribution from inner-shell ionization. Figure 15b shows a more elaborate synthetic spectrum, which also takes into account the charge exchange contributions (hatched areas) between TiXXII and neon, to simulate the spectrum in Fig. 15a. The calculations of this synthetic spectrum are, however, based on assumptions about a 'charge-averaged' charge exchange recombination coefficient the relative abundance of hydrogen- and helium-like titanium ions, n(H)/n(He), and the ratio of the neon and electron densities, n_{Ne}/n_e. We note that the latter quantities were not determined from measurements.

Spectra of TiXXI –TiXX were also observed by Bitter et al. [36] from TFTR tokamak plasmas with a crystal spectrometer of very high spectral resolution ($\lambda/\Delta\lambda = 25000$). The data were analyzed by least-squares fits of synthetic spectra constructed from theoretical predictions. Figure 16 shows an example of the TiXXI –TiXX spectra from TFTR (a) and contributions from the various components, subfigs. 16 (b-c), which were determined from a least squares fit of a synthetic spectrum to the experimental data. The dielectronic and inner-shell collisionally excited lithium-like satellite feature were found to be in excellent agreement with the theoretical predictions – see subfigs. 16(c)-(d), but the intensities of the helium-like lines x, y, and z were much higher than the contributions predicted for direct electron-impact excitation from the ground state – see subfig. 16(b).

Figure 17 presents the experimental values for the intensity ratios x/w, y/w and z/w of the TiXXI spectra from TFTR as a function of the electron temperature for different minor and major plasma radii together with the theoretical predictions for direct electron impact excitation from the ground state and electron impact excitation to levels with $n>2$ including cascading. The intensity ratios observed at low electron temperatures are significantly higher than the theoretical predictions.

We finally also mention the measurements of the satellite spectra of heliumlike nickel on JET [37] and TFTR [38]. The X-ray crystal spectrometer on JET covered a narrow wavelength range 1.585 to 1.595 Å, which included the heliumlike lines w and x, whereas the x-ray crystal spectrometer on TFTR covered the range from 1.585 to 1.6100 Å, which also included the heliumlike lines y and z. However, due to the Z-dependent wavelength shift of the heliumlike lines, the lines y and z in the spectrum of NiXXVII are blended with the lithiumlike and berylliumlike satellites q and β, respectively, so that the intensity of the heliumlike lines y and z must be determined from a least-squares fit of a synthetic spectrum, which contains all the spectral features. Figure 18 shows the experimental data for x/w from a large variety of JET plasmas as a function of the electron temperature and, for comparison, the theoretical predictions for two extreme cases of the electron density and electron temperature profiles. The experimental values for x/w are well above both these theoretical predictions. Contrary to the measurements presented in [37], which covered a large variety of plasma discharges, the measurements on TFTR [38] were performed on a series of 50 discharges with purely Ohmic heating. These plasmas had nearly identical, fairly flat electron density and electron temperature profiles. However, the peak electron density decreased and the peak

electron temperature increased from discharge to discharge. Figure 19 shows the experimental values for the intensity ratios of x/w, y/w, and z/w in NiXXVII, which were obtained from these TFTR plasmas, as a function of the peak electron temperature. The error bars represent the uncertainties of these line ratios, which were obtained from the least-squares fit analysis. The solid lines represent theoretical predictions, where the uppermost line is always the total of the contributions from different excitation processes, which include electron impact excitation of NiXXVII, recombination of NiXXVIII, and inner-shell ionization of NiXXVI. We infer from Fig 19 that the experimental values for all three line ratios are above the theoretical predictions, with the largest deviations occurring at low electron temperatures, which is reminiscent of the Ti XXI results from TFTR shown in Fig. 17.

For completeness we also present results from recent observations of charge exchange recombination on NSTX [39]. Figure 20 shows a sequence of three spectra of helium-like argon, which were recorded from a NSTX plasma discharge during the period from 210 to 250 ms with a time resolution of 10 ms. During the time interval from 220 to 230 ms a short neutral hydrogen beam pulse was injected into the plasma for diagnostic purposes. The spectra, which were obtained during the time intervals from 210 to 220 ms and from 240 to 250 ms – see subfigs. 20(a, c), show in addition to the helium-like lines w, x, y, and z the typical dielectronic and inner-shell, collisionally excited lithium-like satellites, whereas the spectrum in subfig. 20(b), which was obtained during the injection of the neutral hydrogen beam pulse, shows only the helium-like lines w, x, y, and z. This neutral beam pulse changed the ionization balance in the plasma dramatically by charge

exchange recombination. In fact, the helium-like and lithium-like charge states, which are needed to produce the satellite spectra, must have disappeared during the injection of the neutral hydrogen beam pulse, and the helium-like lines w, x, y and z must have been produced by charge-exchange of hydrogen-like argon ions with the injected neutral hydrogen. In the spectrum shown in subfig. 20(b), the lines x, y, and z are stronger than the line w. We may therefore conclude that the line ratios x/w, y/w. and z/w will be enhanced if recombination effects are important. - We point out that the sightline of the X-ray crystal spectrometer on NSTX crossed the direction of the neutral beam, so that the line emission by charge-exchange recombination with the energetic (up to 40 keV/amu) neutral hydrogen beam could be directly observed. – The charge-transfer population of the *high-n* levels in Ar^{+16} from normal hydrogen in the ground and excited states in the periphery of Alcator C-Mod plasmas had been previously observed by Rice et al. [40].

IV. Electron Beam Ion Trap Measurements

The tokamak measurements of the higher-Z helium-like spectra raise the question of the correctness of the theoretical atomic data. A series of measurements were performed at the Electron Beam Ion Trap (EBIT) facility at Livermore to address this question. This series included measurements of the electron-impact excitation cross sections, of the contributions from resonance excitation and radiative cascades, of the dielectronic satellite line resonance strengths, and of the contributions from innershell ionization.

Measurements of the electron-impact excitation cross sections of the w, x, y, and z lines of Ti XXI performed on one of the Livermore electron beam ion traps over a wide range

of electron energies were reported by Chantrenne et al. [41]. These measurements included resonance excitation and radiative cascades and thus provided a comprehensive test of atomic theory. The measurements are described elsewhere in this volume [42], and we only briefly mention that the agreement with theory was very good, i.e., typically better than 10% and thus within the uncertainty of the absolute calibration. Differences larger than this were only obtained for line z, which was measured to be about 20% larger than predicted. By contrast, the above-threshold resonances contributing to the lines were found to be somewhat overpredicted by theory [43].

Because the Ti XXI cross sections were measured over a wide range of energies, the EBIT measurements could be used to calculate the excitation rate coefficient for each line as a function of temperature [41]. A comparison between the G ratio inferred from the EBIT measurements [43] and those calculated by the theory used to compare with the TFTR results in [36] is shown in Fig 21. The agreement between the electron beam ion trap results and theory is very good – even at the lowest electron temperatures, where the TFTR data, by contrast, differed markedly from theory. Additional cross section measurements of the lines in helium-like V XXII, Cr XXIII, Mn XXIV, and Fe XXV performed with the Livermore electron beam ion traps also found very good agreement with atomic theory [44].

Measurements of the dielectronic satellites contributing to the spectra of the helium-like ions have also been conducted [45-47]. Most important for the helium-like lines is to make sure that any blends with dielectronic satellite lines are correctly accounted for,

especially as these satellites increase their relative strength at the lowest temperature where the discrepancies with theory were found to be largest. Good agreement between the measurements and theory has been found. This agreement includes the strength of the dielectronic satellites with a high-n ($n \geq 3$) spectator electron. As noted above, these satellites merge with the *1s - 2p* resonance line w and to a lesser extent with the intercombination line y, as illustrated in Figs. 8 and 9. Measurements at the Livermore electron beam ion traps have resolved these satellites [48], as shown in Fig. 22, and found agreement with theory to within 10 % [49]. This good agreement with theory excludes that blending with unknown satellites can explain the puzzling results observed on tokamaks.

Since at low electron temperatures, where the discrepancy between tokamak data and theory is largest, a large fraction of the ions is in the lithium-like charge state, one may assume that innershell ionization of lithium-like ions may excite the helium-like lines. This process, $1s^2 2s + e^- \rightarrow 1s2s + 2e^-$, however, only leads to the excitation of line z, as illustrated in Fig. 23 [50,51]. Lines x and y do not get enhanced by this process. Measurements of the cross sections for this process using the Livermore electron beam ion traps agree very well with theory [52]. Moreover, the energy needed to ionize the 1s electron is very high (and close to the energy needed to make hydrogen-like ions). At low electron temperature there are very few electrons with the required energy and this process is slow.

Another process, which might enhance the intensity of the helium-like lines when a large fraction of the ions is in the lithium-like charge state was proposed by Yong-Ki Kim [53]. Here the upper levels of the helium-like lines might be populated by excitation from the lithium-like ground state, $1s^2 2s$, to the metastable lithium-like state $1s2s2p\ ^4P_{5/2}$ and the subsequent ionization of this metastable state to *1s2s* and *1s2p*. This process requires much less energy than the innershell ionization process described above, because the binding energy of the *2s* or *2p* electron is much less than that of the *1s* electron. However, the process was not predicted to be likely to occur, because despite its relatively long-lived nature, the metastable lithium-like state $1s2s2p\ ^4P_{5/2}$ was predicted to decay both by autoionization and by x-ray emission before ionization of one of the $n = 2$ electrons could occur.

To further investigate the importance of the process suggested by Yong-Ki Kim two experiments were conducted at the electron beam ion traps in Livermore, using the spectra of helium-like iron, FeXXV, as an example. In the first experiment, the energy of the electron beam was varied from 5600 to 8500 eV, so that only the helium-like lines w, x, y, z and the dielectronic satellites *1s2lnl'* with $n \geq 3$ could be excited – see Fig. 24 . In the second experiment, the energy of the electron beam was varied from 4700 to 8500 eV, so that the helium-like lines w, x, y, z and all the associated dielectronic and inner-shell, collisionally excited, satellites *1s2lnl'* with $n \geq 2$ could be observed – see Fig. 25. Here, the electron beam was kept at the energy of 4700 eV for an extended period of time to enhance the density of ions in the lithium-like ground state. An overlay of the spectra obtained from these two experiments is shown in Fig. 26. We note that the intensities of

the helium-like lines are essentially the same in both spectra, even though the intensity of satellite q, which was produced by inner-shell excitation from the lithium-like ground state and which is therefore a measure of the concentration of the lithium-like ions, was very high in the spectrum obtained from the second experiment. We must therefore conclude that the mechanism proposed by Yong-Ki Kim, does not play an important role for the excitation of the helium-like lines, at least not for iron and the densities of electron beam ion trap plasmas. We should note that the direct x-ray decay of the metastable lithium-like state $1s2s2p\ ^4P_{5/2}$ has now been detected in the collisional satellite spectrum of Ar XVII both at the Livermore electron beam ion traps and the Princeton NSTX spherical torus [54], making it less plausible that this state can play a role in enhancing lines x, y, and z.

V. Discussion

We reiterate that in all tokamak experiments except for the DITE experiments, where the R and G ratios were in good – or excellent – agreement with the theoretical predictions, the line ratios x/w, y/w, and z/w were found to be significantly higher than predicted, yet at the same time EBIT measurements revealed no comparable discrepancies with theory. Keenan et al. point out, that their results are applicable only when the atomic processes in the plasma are appropriate to the core region where ion diffusive time scales are long compared to the time to reach ionization equilibrium [34]. This comment may yield the key to a solution of the riddle posed by the disparate results from various tokamak experiments, since it is questionable that the above mentioned conditions were fulfilled in

all tokamak experiments. In ref. [33] Keenan et al. explored the radial dependence of the emissivity for the helium-like SiXIII lines, showing spectra from different radial chords that were obtained by a radial scan of their spectrometer. They observed an enhancement of the line z over the line w in the cooler outer regions of the plasma, which they ascribed to the recombination of hydrogen-like ions that were moved from the core to the outer regions of the plasma by radial transport. – Such an enhancement of the line z on outer radial chords was also observed on Alcator C-Mod [55]. - From an examination of the emission profiles they concluded that almost all the SiXIII line emission was from the central part of the DITE plasmas and that 'the R and G ratios could be measured from a central-chord integrated signal alone' [34]. It seems that all other tokamak experiments were based on the same conclusion, however, without a proper justification by profile measurements as in the case to the DITE experiments. Fortunately, there is hope that new instrumental developments will soon improve the state of the art in the X-ray spectroscopy of extended *tokamak-like* fusion plasmas. These new developments, which are briefly described in the following section, will provide us with better tools to address the complexity of atomic processes in tokamak plasmas.

VI. Recent Advances in the X-ray spectroscopy of tokamak plasmas.

The spectra of highly charged ions in tokamak plasmas have up to now been observed with single-chord X-ray crystal spectrometers, which provided data from only a single - usually a central - sightline through the plasma. In a few tokamak experiments, information on the radial profiles of line emissivities was obtained by moving a single-chord spectrometer to different radial positions between discharges and keeping the

plasma parameters from discharge to discharge as constant as possible. Also radial arrays of several (up to five) single-chord spectrometers were occasionally used, as on TFTR and Alcator C-Mod. However, with both methods one could get only coarse information on the radial profiles of the line emissivities, so that it was generally not possible to determine the contributions from the various processes of line excitation with sufficient accuracy. This situation has now changed thanks to the advent of a new type of X-ray imaging crystal spectrometer, which can provide spatially resolved spectra from a large number of sightlines through the plasma simultaneously with a time resolution of a few ms. The spectrometer consists of a spherically bent crystal and a two-dimensional position-sensitive detector; the working principle and results from a proof-of-principle experiment on Alcator C-Mod are described in refs. [56] and [57]. Recently, a new X-ray imaging crystal spectrometer, which is equipped with new pixellated semiconductor detectors of a very high photon count rate capability of 1 MHz per pixel, has been installed on Alcator C-Mod [58]. The spectrometer records spectra from the entire height (72 cm) of the elongated plasma cross-section with a spatial resolution in the plasma of about 1 cm. Figure 27 shows a surface plot of spatially resolved helium-like argon spectra, which were obtained from an Alcator C-Mod tokamak discharge with this new instrument. We infer from Fig. 27 that the spectra from the central part and the outer regions of the plasma are distinctly different: The spectra, which are emitted from the central region of the plasma, consist of the helium-like argon lines and the associated lithium-like satellites, whereas the spectra emitted from the colder edge region of the plasma consist only the four helium-like argon lines w, x, y, and z, of which the line z is the strongest and the line w the weakest feature. The helium-like lines in the outer region

of the plasma must have been produced by recombination of hydrogen-like argon ions. Since the electron density of Alcator C-Mod plasmas is about a factor 10 higher than in other tokamak experiments, one would expect the ion charge state distribution to be close to coronal equilibrium. To find hydrogen-like argon ions far out in the cold edge region of Alcator C-Mod plasmas was therefore a rather unexpected observation. We are presently developing an algorithm to determine the local line emissivities by an inversion of the line-integrated spectral data shown in Fig. 27. The algorithm applies to elongated (bean-shaped) plasma cross-sections and can be considered as an expansion of the Abel inversion, which applies to a circular plasma cross-section. One of our next projects will be to reevaluate the helium-like satellite spectra and the line ratios x/w, y/w, and z/w as a function of the minor plasma radius. These data should provide the most definitive tests yet of the correctness of the modeling of tokamak spectra.

Acknowledgments

Work by the Princeton University Plasma Physics Laboratory was performed under the auspices of the Department of Energy under Contract No. DE-AC02-76CHO3073; work by the University of California Lawrence Livermore National Laboratory was performed under the auspices of the Department of Energy under Contract No. W-7405-Eng-48; the work at Massachusetts Institute of Technology was supported by the Department of Energy contract No. DE-FC02-99ER54572 and the Department of Energy Initiative for the Development of Diagnostics for Magnetic Fusion Energy Research Contract-1083.

References

(1) E. P. Garbunov, D. P. Ivanov, N. J. Peacock, D. C. Robinson, V. Strekov, *in Proceedings of the 4th European Conference on Controlled Fusion and Plasma Physics, Rome Italy, August 31 – September 4, 1970; p. 19*

(2) S. von Goeler et al, Nucl. Fusion **15**, 301 (1975)

(3) M. J. Seaton and P. J. Storey, in Atomic Processes and Applications, edts. P. G. Burke and B. L. Moiseiwitsch, North-Holland Publishing Company, Amsterdam, New York, Oxford, p. 133 – 197, 1976

(4) S. von Goeler, European Conference on Controlled Fusion and Plasma Physics, Lausanne, September 1-5, 1975, Vol. II, p. 71 – 73.

(5) K. W. Hill, et al., Phys. Rev. A **19**, 1770 (1979)

(6) H. Johann, Z. Phys.**69**, 185 (1931)

(7) M. Bitter, et al., Phys. Rev. Lett. **42**, 304 (1979)

(8) A. H. Gabriel, Mon. Not. R. Astr. Soc. **160**, 99 (1972)

(9) C. P. Bhalla, et. al., Mon. Not. R. Astr. Soc. **172**, 359 (1975)

(10) L. A. Vainstein and U. I. Safronova, Atomic Data and Nuclear Data Tables **21**, 49 (1978)

(11) F. Bely-Dubau, et al., Mon. Not. R. Astr. Soc. **186**, 405 (1979)

(12) F. Bely-Dubau, et al., Mon. Not. R. Astr. Soc. **189**, 801 (1979)

(13) F. Bely-Dubau, et al., Mon. Not. R. Astr. Soc. **198**, 239 (1982)

(14) M. Bitter, et al., **43**, 129 (1979)

(15) P. Beiersdorfer, *'High-resolution studies of the X-ray transitions in highly charged neonlike ions on the PLT tokamak', Ph. D. Dissertation 1988, Princeton University*

(16) G. Bertschinger, O. Marchuk, TEXTOR Team, Fusion Science and Technology, **47**, 253 (2005)

(17) N. P. Basse, A. Dominguez, E. M. Edlund, et al., Fusion Science and Technology, **51**, 476 (2007)

(18) B. C. Stratton, M. Bitter, K. W. Hill, D. L. Hillis, and J. T. Hogan, *accepted for publication in* Fusion Science and Technology

(19) K. W. Hill, M. Bitter, M. Tavernier, M. Diesso, S. von Goeler, G. Johnson, L. C. Johnson, N. R. Sauthoff, N. Schechtman, S. Sesnic, F. Tenney, and K. M. Young, Rev. Sci. Instrum. **56**, 848 (1985)

(20) M. Bitter, K. W. Hill, S. Cohen, S. von Goeler, H. Hsuan, L. C. Johnson, R. Raftopulos, M. Reale, N. Schechtman. S. Sesnic, F. Spinos, J. Timberlake, S. Weicher, N. Young, and K. M. Young, Re, Sci. Instrum. **57**, 2145 (1986)

(21) M. Bitter, H. Hsuan, J. E. Rice, K. W. Hill, M. Diesso, B. Grek, R. Hulse, D. W. Johnson, L. C. Johnson, and S. von Goeler, Rev. Sci. Instrum. **59**, 2131 (1988)

(22) R. Bartiromo, F. Bombarda, R. Giannella, S. Moantovani, L. Panccione, and G. Pizzicaroli, Rev. Sci. Instrum. **60**, 237 (1989)

(23) M. Bitter, H. Hsuan, K. W. Hill, and M. Zarnstorff, Physica Scripta **T47**, 87 (1993)

(24) F. Bely-Dubau, J. Dubau, P. Faucher, and A. H. Gabriel, Mon. Not, R. Astron. **198**, 239 (1982)

(25) M. Bitter and TFTR Group, Plasma Physics and Controlled Fusion **29**,1235 (1987)

(26) A. H. Gabriel and Carole Jordan, Mon. Not. R. astr. Soc. **145**, 241 (1969)

(27) C. D. Lin, W. R. Johnson, and A. Dalgarno, Phys. Rev. A, **15**, 154 (1977)

(28) RWP McWhirter, proceedings *Course on Plasma Diagnostics and Data acquisition Systems, Varenna – Villa Monastero – Italy, September 3-11, 1975, p. 178 – 243, edited by A. Eubank and E. Sindoni, Bologna*

(29) O. Bely, Phys. Lett. **26A**, 408 (1968)

(30) A. Burgess, D. G. Hummer, J. A. Tully, Phil. Trans. Roy. Soc. **266**, 225 (1970)

(31) F. P. Keenan, S. M. McCann, and A. E. Kingston, Phys. Scr. **35**, 432 (1987)

(32) P. G. Burke and W. D. Robb, Adv. At. Mol. Phys. **11**,143 (1975)

(33) F. P. Keenan, S. M. McCann, R. Barnsley, J. Dunn, K. D. Evans, and N. J. Peacock, Phys. Rev. A **39**, 4092 (1989)

(34) F. P. Keenan, S. M. McCann, A. E. Kingston, R. Barnsley, J. Dunn, N. J. Peacock, Phys. Rev. A **44**, 3831 (1991)

(35) T. Kato, S. Morita, K. Masai, and S. Hayakawa, Phys. Rev. A **36**, 795 (1987)

(36) M. Bitter, K. W. Hill, M. Zarnstorff, S. von Goeler, R. Hulse, L. C. Johnson, N. R. Sauthoff, S. Sesnic, K. M. Young, M. Tavernier, F. Bely-Dubau, P. Faucher, M. Cornille, and J. Dubau, Phys. Rev. A **32**, 3011 (1985)

(37) K. –D. Zastrow, E. Källne, and H. P. Summers, Phys. Rev. A **41**, 1427 (1990)

(38) M. Bitter, H. Hsuan, V. Decaux, B. Grek, K. W. Hill, R. Hulse, L. A. Kruegel, D. Johnson, S. von Goeler, and M. Zarnstorff, Phys. Rev. A **44**, 1796 (1991)

(39) P. Beiersdorfer, M. bitter, M. Marion, and R. E. Olson, Phys. Rev. A **72**, 032725 (2005)

(40) J. E. Rice, E. S. Marmar, J. L. Terry, E. Källne, and J. Källne, Phys. Rev. Lett. **56**, 50 (1986)

(41) S. Chantrenne, P. Beiersdorfer, R. Cauble and M. Schneider Phys. Rev. Lett. **69**, 265 (1992).

(42) H. Chen and P. Beiersdorfer, Canadian Jorunal of Physics (this issue).

(43) P. Beiersdorfer, R. Cauble, S. Chantrenne, M. H. Chen, N. DelGrande, D. A. Knapp, R. E. Marrs, A. Osterheld, K. Reed, M. B. Schneider, J. Scofield, B. Wargelin, K. Wong, D. A. Vogel, and R. Zasadzinski, in *UV and X-Ray Spectroscopy of Astrophysical and Laboratory Plasmas*, edited by E. Silver and S. Kahn (Cambridge, 1993), p. 59-68.

(44) K.L. Wong, P. Beiersdorfer, K.J. Reed, and D.A. Vogel, Phys. Rev. A **51**, 1214 (1995)

(45) P. Beiersdorfer, M. H. Chen, R. E. Marrs, M. B. Schneider, R. S. Walling, Phys. Rev. A **44**, 396 (1991)

(46) P. Beiersdorfer, T. W. Phillips, K. L. Wong, R. E. Marrs, D. A. Vogel, Phys. Rev. A **46** 3812 (1992)

(47) A. J. Smith, P. Beiersdorfer, V. Decaux, K. Widmann, A. Osterheld, M. Chen, Physical Review A **51**, 2808 (1995)

(48) P. Beiersdorfer, M. B. Schneider, M. Bitter, and S. von Goeler, Review of Scientific Instruments **63**, 5029 (1992)

(49) P. Beiersdorfer, Annual Review of Astronomy and Astrophysics **41**, 343 (2003)

(50) P. Beiersdorfer, in *X-Ray and Inner-Shell Processes, Knoxville, TN 1990*, AIP Conf. Proc. No. 215, edited by T. A. Carlson, M. O. Krause, and S. T. Manson (AIP, NY 1990) 648-658.

(51) D. A. Vogel, P. Beiersdorfer, R. E. Marrs, K. L. Wong, R. Zasadzinski, Zeitschrift f. Physik D **21**, S193 (1991).

(52) D. A. Vogel, *'Electron Impact Ionization of Highy charged Lithiumlike Ions', Ph. D. Dissertation 1992, Georgia Institute of Technology.*

(53) Yong-Ki Kim, *private communication*

(54) P. Beiersdorfer, M. Bitter, D. Hey, and K. J. Reed, Physical Review A **66**, 032504 (2002)

(55) J. E. Rice, E. S. Marmar, E. Källne, and J. Källne, Phys. Rev. A, **35**, 3033 (1987)

(56) M. Bitter, K. W. Hill, A. L. Roquemore, P. Beiersdorfer, S. M. Kahn, S. R. Elliott, and B. Fraenkel, Rev. Sci. Instrum. **70**, 292 (1999)

(57) M. Bitter, K. W. Hill, B. Stratton, A. L. Roquemore, S. G. Lee, J. G. Bak, M. K. Moon, U. W. Nam, G. Smith, J. E. Rice, P. Beiersdorfer, and B. S. Fraenkel, Rev. Sci. Instrum. **75**, 3660 (2004)

(58) *The X-ray imaging crystal spectrometer on Alcator C-Mod was built in collaboration with J. E Rice and A. Ince-Cuhman from the Massachusetts Institute of Technology and M. Bitter and K. W. Hill from the Princeton Plasma Physics Laboratory. It is in operation since April 2007. The instrumental details will be described in a forthcoming paper.*

TABELS:

TABLE I: Experimental wavelengths and theoretical wavelengths for spectral features shown in Fig. 5 from (a) A. H. Gabriel, Mon. Not Roy. Astron. Soc. **160**, 99 (1972), (b) A. M. Ermolaev, et al. Astrophys. Lett. **12**, 53 (1972), and (c) L. A. Vainshtein and U. I. Safronova, Sov. Astron. – AJ **15**, 175 (1971)

	Transition	λ_{expt} (Å)	λ_{theor} (Å)
w	$1s^2(^1S_0) - 1s2p\,(^1P_1^\circ)$	1.8500	1.8500[a]
			1.84992[b]
x	$1s^2(^1S_0) - 1s2p\,(^3P_2^\circ)$	1.8552	1.8551[a]
			1.85519[b]
t	$1s^22s(^2S_{1/2}) - 1s2p\,2s(^2P_{1/2}^\circ)$	1.8567	1.8570
y	$1s^2(^1S_0) - 1s2p\,(^3P_1^\circ)$	1.8592	1.8591[a]
			1.85947[b]
q	$1s^22s(^2S_{1/2}) - 1s2p\,2s(^2P_{3/2}^\circ)$	1.8608	1.8604[a]
a	$1s^22p\,(^2P_{3/2}^\circ) - 1s2p^2(^2P_{3/2})$	1.8618	1.8618[a]
k	$1s^22p\,(^2P_{1/2}^\circ) - 1s2p^2(^2D_{3/2})$	1.8632	1.8631[a]
r	$1s^22s(^2S_{1/2}) - 1s2p\,2s(^2P_{1/2}^\circ)$		1.8635[a]
j	$1s^22p\,(^2P_{3/2}^\circ) - 1s2p^2(^2D_{5/2})$	1.8657	1.8657[a]
z	$1s^2(^1S_0) - 1s2s(^3S_1)$	1.8681	1.8677[a]
			1.86801[b]
β	$1s^22s^2(^1S_0) - 1s2s^22p\,(^1P_1)$	1.8705	1.8710[c]

TABLE II: Results from least squares fits to spectra shown in Figs. 8 and 9, columns A and B, respectively.

Parameters	Spectrum A	Spectrum B
Ti (keV)	3.2 ± 0.1	20.7 ± 0.3
Te (keV)	3.29± 0.04	8.2 ± 0.04
N_{Li} / N_{He}	0.376± 0.012	0.260± 0.008
N_{Be} / N_{He}	0.144± 0.013	0.018± 0.005
xa *(multiplier)*	1.59± 0.05	2.49± 0.08
ya *(multiplier)*	1.61± 0.04	1.80± 0.04
za *(multiplier)*	1.65± 0.04	2.29± 0.06

Tabel III: Rates for radiative transitions from the $n = 2$ levels of helium-like ions in sec^{-1}
New version: Lin-Dalgarno-table.doc **ref [27]**

Element /Atomic Number Z	$2\ ^1P_1 - 1\ ^1S_0$ (*E1*)	$2\ ^3P_1 - 1\ ^1S_0$ (*E1*)	$2\ ^3P_2 - 1\ ^1S_0$ (*M2*)	$2\ ^3P_2 - 2\ ^3S_1$ (*E1*)	$2\ ^3S_1 - 1\ ^1S_0$ (*M1*)
8 O	3.30(12)	5.56(8)	3.33(5)	8.31(7)	1.06(3)
12 Mg	1.95(13)	3.40(10)	1.06(7)	1.52(8)	7.33(4)
14 Si	3.76(13)	1.58(11)	3.89(7)	2.00(8)	3.61(5)
18 Ar	1.07(14)	1.82(12)	3.16(8)	3.61(8)	4.80(6)
22 Ti	2.41(14)	1.06(13)	1.66(9)	7.07(8)	3.76(7)
26 Fe	4.59(14)	4.26(13)	6.55(9)	1.47(9)	2.08(8)
28 Ni	6.06(14)	7.49(13)	1.20(10)	2.17(9)	4.45(8)

Figure Captions

Figure 1: A typical X-ray spectrum from the ST tokamak, exhibiting a thermal continuum, impurity K and L lines of limiter and wall material (molybdenum, iron, chromium, and nickel), and a high-energy tail produced by runaway electrons. The spectrum was measured with the lithium-drifted silicon detector of a Pulse-Height Analysis system which is shown in the insert, using a set of apertures and Be- and Al-filters to select energy range and photon flux.

Figure 2: Kα-line structure of iron: a) spectrum measured on ST at a central electron temperature of 1200 eV; b) computations of the Kα-line structure by Cowan, including the contributions from direct excitation and dielectronic recombination.

Figure 3: Schematic of the Johann X-ray crystal spectrometer on the PLT tokamak, consisting of a cylindrically bent Ge (220) crystal and a position-sensitive multi-wire proportional counter.

Figure 4: Line profiles of the FeXXV $1s^2$ (^1S)-1s2p ($^1P_1$) resonance line (a) before and (b), (c) during neutral beam injection, in time intervals of 50 ms (conversion: 0.18 eV/channel); and ion-temperature derived from the Doppler broadening of these line profiles as a function of time.

Figure 5: Dielectronic satellite spectrum of FeXXV recorded from PLT for central electron temperatures of 1.65 keV (a) and 2.30 keV (b) (conversion: 0.18 eV/channel). The lines have been identified, using notation of A. H. Gabriel, Mon. Not Roy. Astron. Soc. **160**, 99 (1972). The solid curves represent least-squares fits of Voigt functions to the most prominent peaks.

Figure 6: Observed and predicted line ratios with respect to the resonance line ***w*** as a function of the electron temperature (Te) for (a) dielectronic satellite ***j***; (b) intercombination ***(x, y)*** and forbidden ***(z)*** lines. - The dashed lines were only drawn to aid the eye. - The theoretical predictions for Te = 2.7 keV are: ***x/w*** = 0.35, ***y/w*** = 0.25, ***z/w*** = 0.41; (c,d) inner-shell excited lithium- and beryllium-like satellites ***q*** and ***β***. The solid line (1) and (2) represent theoretical predictions for coronal equilibrium by C. Jordan, Mon. Not. Roy. Astron. Soc. **142**, 501 (1969) and H. P. Summers, Mon. Not. Roy. Astron. Soc. **169**, 663 (1974), respectively. Deviations from coronal equilibrium are expected in tokamak plasmas as a result of ion transport.

Figure 7: Central ion temperature from Doppler measurements of the FeXXV resonance line ***w*** as a function of time from a TFTR plasma with 1 MW of Ohmic heating and 20 MW of auxiliary heating by neutral beam injection during the time interval from 3.0 to 4.0 s.

Figure 8: Satellite spectrum of FeXXV. The experimental data (circles) were recorded from the same discharge as in Fig. 7 during the period of Ohmic heating from 2.5 to 3.0 s. Also shown is a synthetic spectrum with its various components (solid lines),

which was constructed from a least-squares fit of theoretical predictions [Bely-Dubau, and Vainshtein] to the experimental data.

Figure 9: Satellite spectrum of FeXXV recorded from the same discharge as in Fig. 7 during the period of neutral-beam injection from 3.5 to 4.0 s. The solid lines represent the least squares-fit of a synthetic spectrum and its components from theoretical predictions.

Figure 10: Table with results from least-squares fit of synthetic spectra from theoretical predictions to the observed spectra in Figs. 8 and 9.

Figure 11: Radial electron temperature profile measured by Thomson scattering, from the same discharge as in Fig. 7

Figure 11: Experimental values and theoretical predictions for the emission line ratio ***R*** as a function of electron density N_e. The theoretical predictions are for the temperature of maximum Mg XI emissivity, $T_m = 7\text{x}10^6$ K with dielectronic and radiative recombination included (solid line) or excluded (dashed line).

Figure 12: Density dependence of helium-like lines of OVII from ref. [28]

Figure 13: Experimental values and theoretical predictions for the ***R*** and ***G*** ratios for the SiXIII helium-like lines of function of electron density and temperature, respectively – from ref. [33].

Figure 14: Experimental values and theoretical predictions for the ***R*** and ***G*** ratios for the MgXI helium-like lines of function of electron density and temperature, respectively – from ref. [34].

Figure 15: Observed satellite spectra of TiXXI (points) and calculated synthetic spectra (solid line) from a JIPP-T-II-U plasma with Ohmic heating and neon puffing. Note: the strong enhancement of the intercombination lines (***x, y***) near channel 200.

Figure 16: Example of an observed TiXXI satellite spectrum from TFTR (a) and contributions from various spectral components: the helium-like lines (b), dielectronic satellites (c) and inner-shell, collisionally excited lithium-like satellites (d), which were obtained from a least-squares fit of a synthetic spectrum. The cross-hatched areas under x, y, and z represent the contributions predicted for electron-impact excitation from the helium-like ground state. The dotted areas under x, y, and z represent the least squares fit of an enhancement factor, with respect to electron impact excitation, to the experimental data.

Figure 17: Observed intensity ratios x/w, y/w and z/w as a function of the central electron temperature for different minor and major plasma radii. Also shown are the theoretical predictions for direct electron impact excitation from the ground state (solid

lines) and electron impact excitation to levels with $n>2$ including cascading (dashed lines).

Figure 18: Line ratio x/w for NiXXVII from JET as a function of the central electron temperature – from ref. [38].

Figure 19: Line ratios x/w, y/w, and z/w for NiXXVII from TFTR as a function of the central electron temperature – from ref. [39].

Figure 20: Sequence of three spectra of helium-like ArXVII from NSTX. The spectra were recorded during the period from 210 to 250 ms of a discharge with a time resolution of 10 ms. A short neutral hydrogen beam pulse was injected during the time interval from 220 to 230 ms.

Figure 21: Comparison of measured and calculated values of the G ratio of the triplet lines ($x+y+z$) to the singlet line w in heliumlike Ti XXI as a function of electron temperature. The calculated values are from [36]. The measured values are from the Livermore electron beam ion traps. (Adapted from Ref. [43].)

Figure 22: Contributions of the dielectronic satellite transitions to the spectrum of Fe XXV. Top: Fe XXV spectrum measured on the Livermore EBIT facility at an electron energy above threshold for electron-impact excitation. Bottom: Measured contributions of the high-n dielectronic satellite transitions with $n = 3, 4, 5,$ and $n \geq 6$.

Figure 23: FeXXV spectrum from the Livermore EBIT with (dashed line) and without (solid line) strong innershell ionization contribution. The experimental conditions for both spectra are the same, except that the ionization balance was adjusted to produce a lot (dashed line) and a small (solid line) fraction of lithiumlike iron, as indicated by the intensity of the Fe XXIV resonance line q.

Figure 24: FeXXV spectrum from the Livermore EBIT for an energy scan of the electron beam from 5600 to 8500 eV. In this energy range only the helium-like lines w, x, y, z and the $n \geq 3$ dielectronic satellites are excited.

Figure 25: FeXXV spectrum from the Livermore EBIT for an energy scan of the electron beam from 4700 to 8500 eV. In this energy range only the helium-like lines w, x, y, z and all the satellites with the $n \geq 2$ are excited.

Figure 26: Overlay of the two spectra from Figs 18 and 19. The spectra have been normalized to each other, using the line w.

Figure 27: Surface plot of spatially resolved ArXVII from Alcator C-Mod. The spectra were recently obtained with a new X-ray imaging crystal spectrometer – see ref. [43]

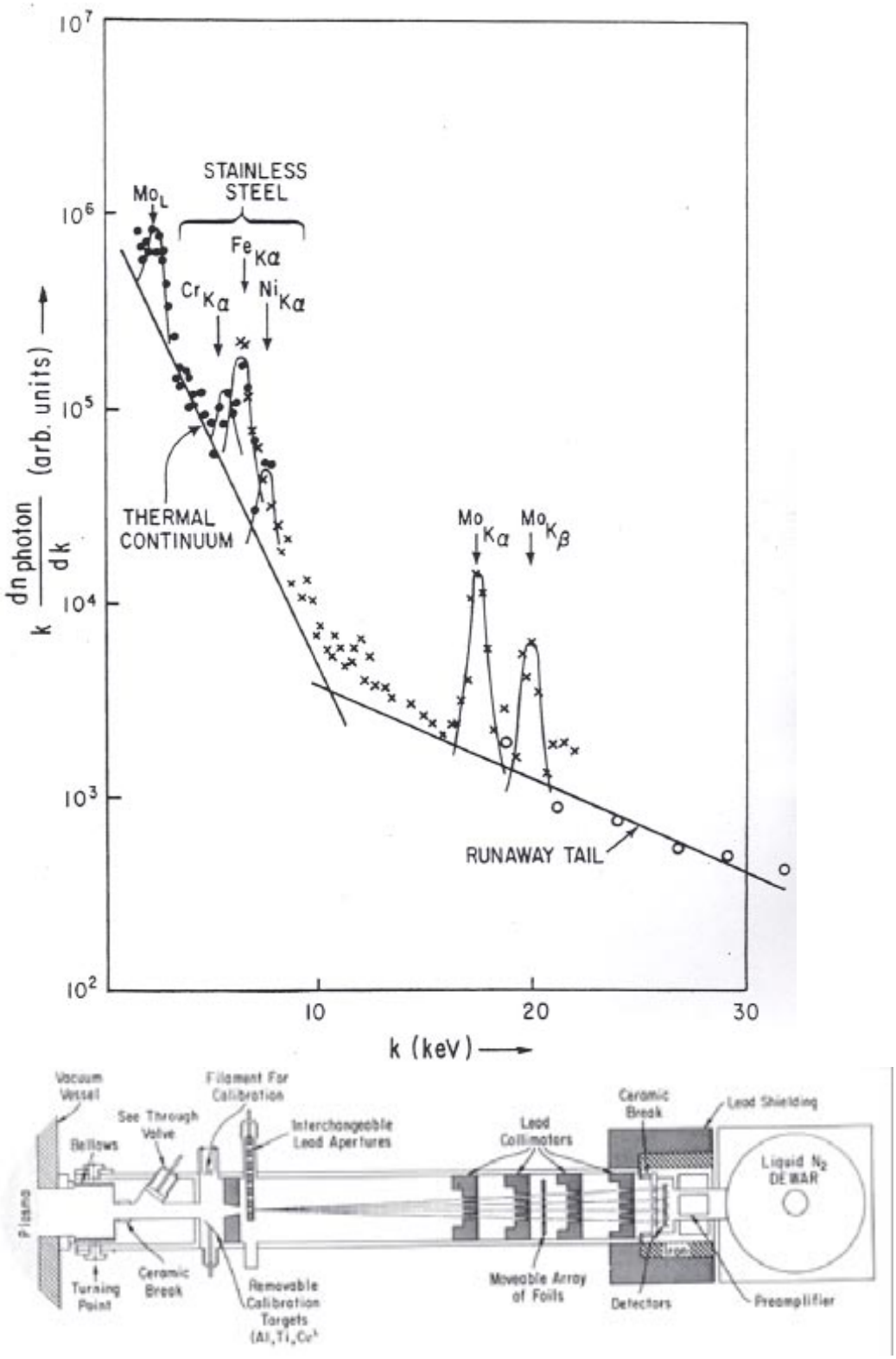
STAINLESS STEEL
Mo L
Fe Kα
Cr Kα
Ni Kα
THERMAL CONTINUUM
Mo Kα
Mo Kβ
RUNAWAY TAIL
k dn photon / dk (arb. units)
k (keV)
Vacuum Vessel
Filament For Calibration
See Through Valve
Bellows
Interchangeable Lead Apertures
Lead Collimators
Ceramic Break
Lead Shielding
Liquid N2 DEWAR
Plasma
Turning Point
Ceramic Break
Removable Calibration Targets (Al, Ti, Cu)
Moveable Array of Foils
Detectors
Preamplifier

Figure 1

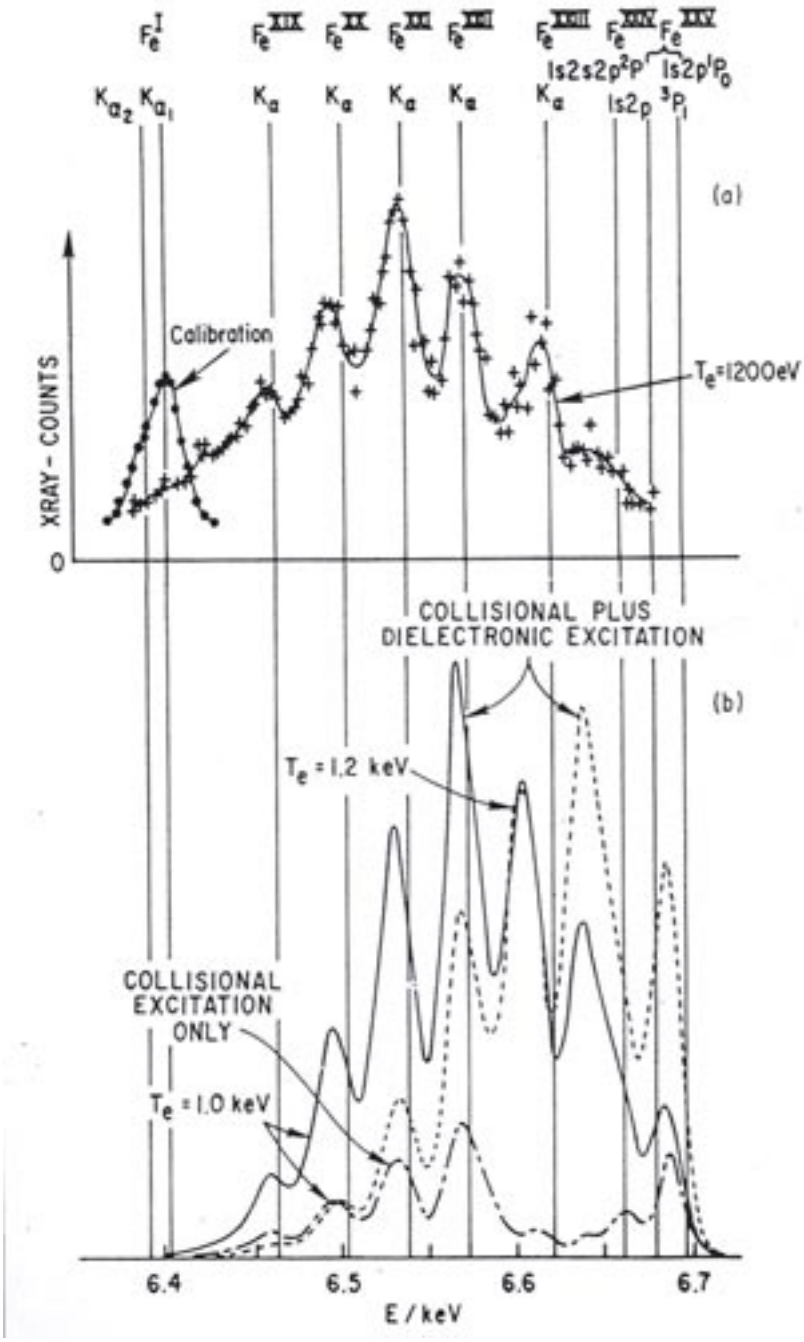
Fe I
Fe XIX
Fe XX
Fe XXI
Fe XXII
Fe XXIII
Fe XXIV
Fe XXV
Is2s2p²P
Is2p¹P₀
Kα₂ Kα₁
Kα
Kα
Kα
Kα
Kα
Is2p ³P₁
(a)
Calibration
Te=1200eV
XRAY - COUNTS
0
COLLISIONAL PLUS
DIELECTRONIC EXCITATION
(b)
Te = 1.2 keV
COLLISIONAL
EXCITATION
ONLY
Te = 1.0 keV
6.4
6.5
6.6
6.7
E / keV

Figure 2

Curved Crystal Spectrometer

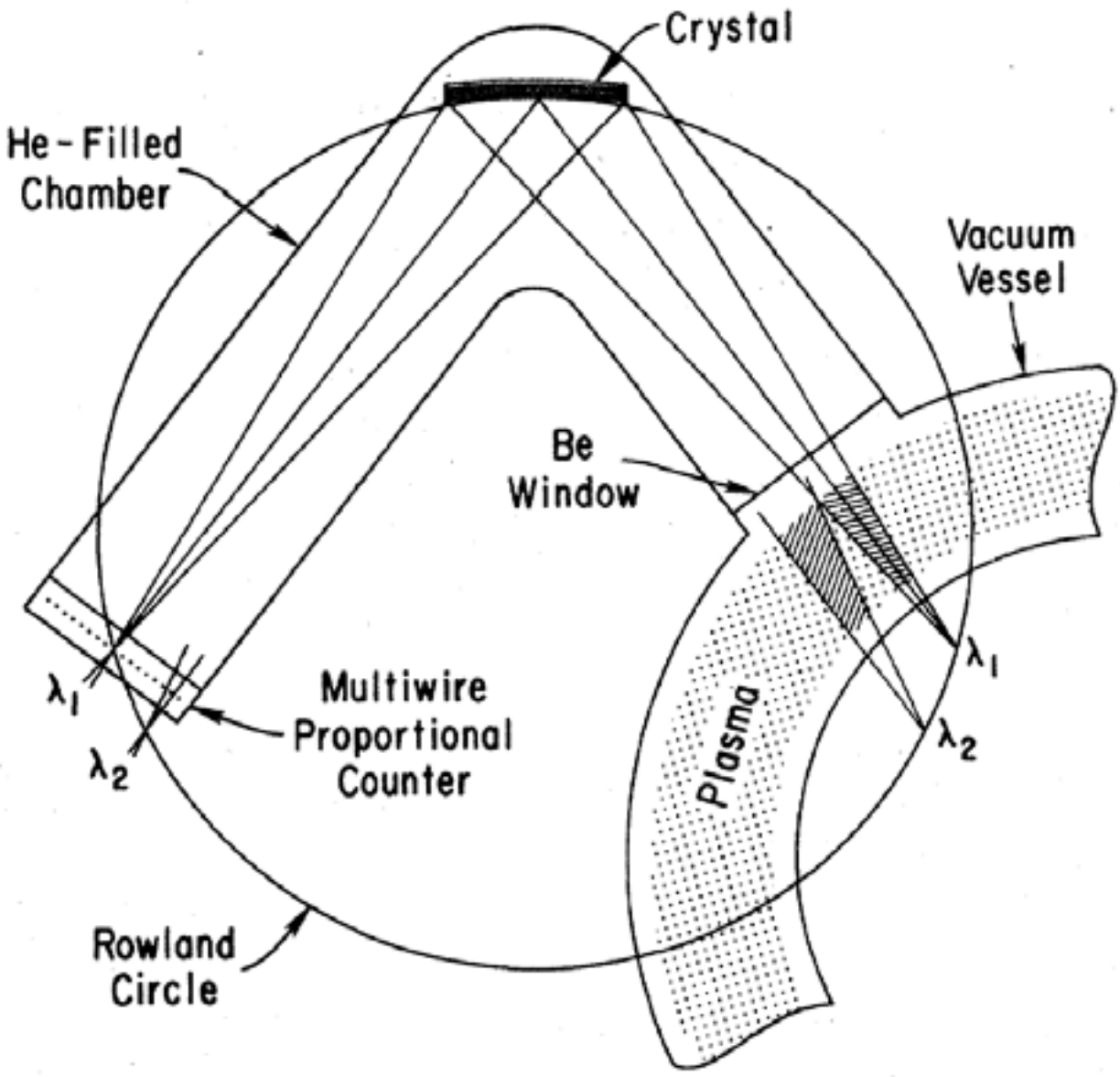

Fig. 3

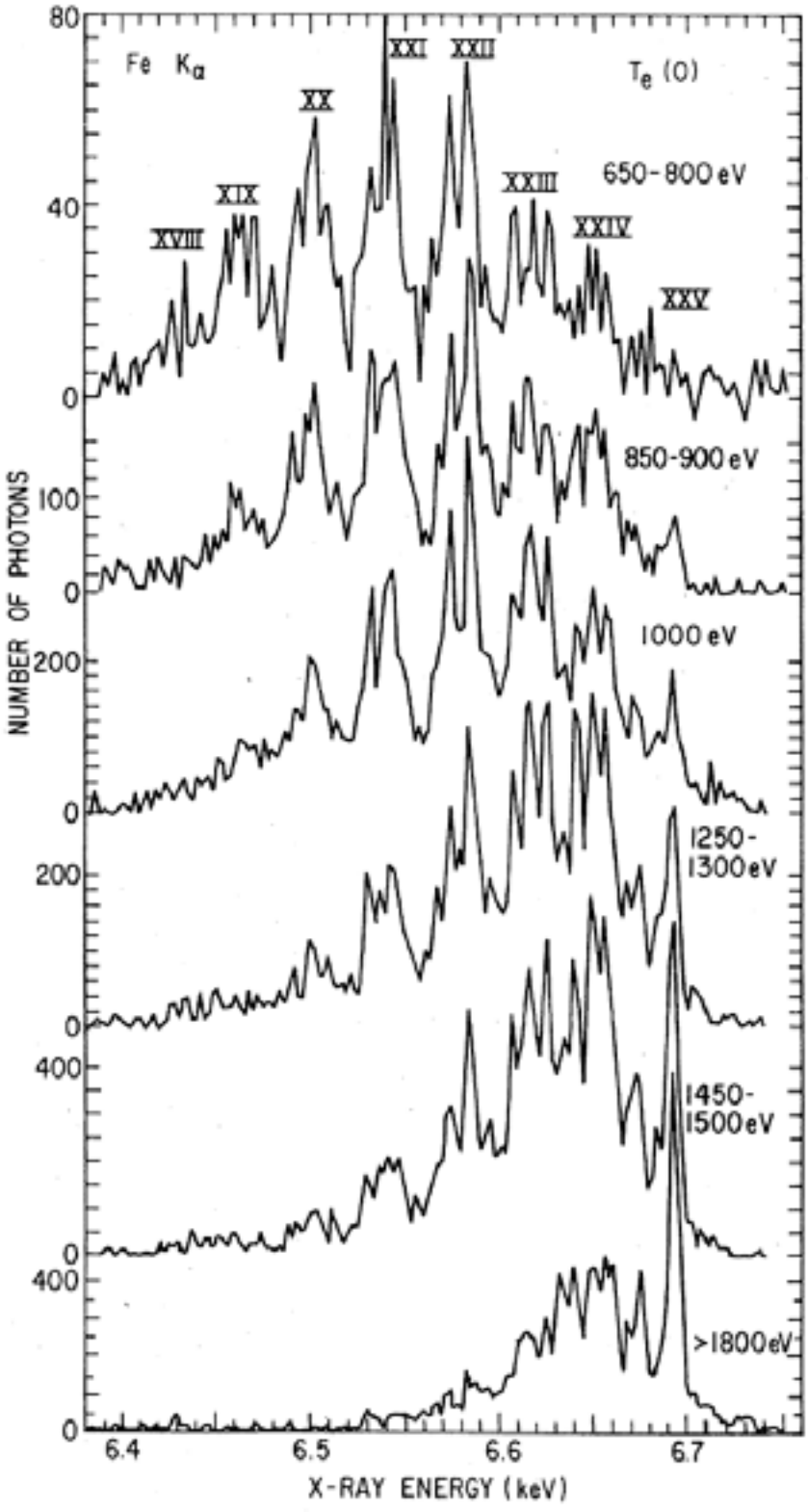
Fe Kα
T_e (0)
650-800 eV
850-900 eV
1000 eV
1250-1300 eV
1450-1500 eV
>1800 eV
XVIII
XIX
XX
XXI
XXII
XXIII
XXIV
XXV
NUMBER OF PHOTONS
X-RAY ENERGY (keV)
6.4
6.5
6.6
6.7
80
40
0
100
0
200
0
200
0
400
0
400
0

Figure 4

Satelllite Spectra of FeXXV from PLT

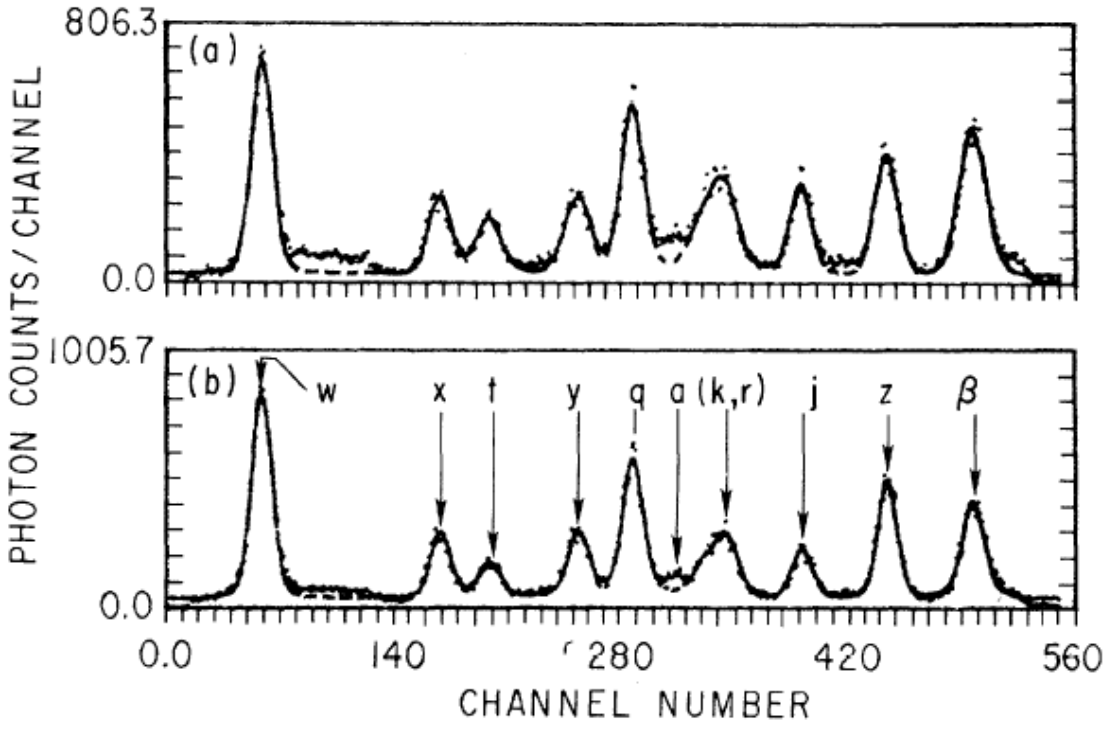

	Transition	λ_{expt} (Å)	λ_{theor} (Å)
w	$1s^2(^1S_0) - 1s2p\,(^1P_1^\circ)$	1.8500	1.8500[a]
			1.84992[b]
x	$1s^2(^1S_0) - 1s2p\,(^3P_2^\circ)$	1.8552	1.8551[a]
			1.85519[b]
t	$1s^22s\,(^2S_{1/2}) - 1s2p\,2s\,(^2P_{1/2}^\circ)$	1.8567	1.8570
y	$1s^2(^1S_0) - 1s2p\,(^3P_1^\circ)$	1.8592	1.8591[a]
			1.85947[b]
q	$1s^22s\,(^2S_{1/2}) - 1s2p\,2s\,(^2P_{3/2}^\circ)$	1.8608	1.8604[a]
a	$1s^22p\,(^2P_{3/2}^\circ) - 1s2p^2(^2P_{3/2})$	1.8618	1.8618[a]
k	$1s^22p\,(^2P_{1/2}^\circ) - 1s2p^2(^2D_{3/2})$	1.8632	1.8631[a]
r	$1s^22s\,(^2S_{1/2}) - 1s2p\,2s\,(^2P_{1/2}^\circ)$		1.8635[a]
j	$1s^22p\,(^2P_{3/2}^\circ) - 1s2p^2(^2D_{5/2})$	1.8657	1.8657[a]
z	$1s^2(^1S_0) - 1s2s\,(^3S_1)$	1.8681	1.8677[a]
			1.86801[b]
β	$1s^22s^2(^1S_0) - 1s2s^22p\,(^1P_1)$	1.8705	1.8710[c]

Figure 5

Analysis of FeXXV Spectra from PLT

Figure 6

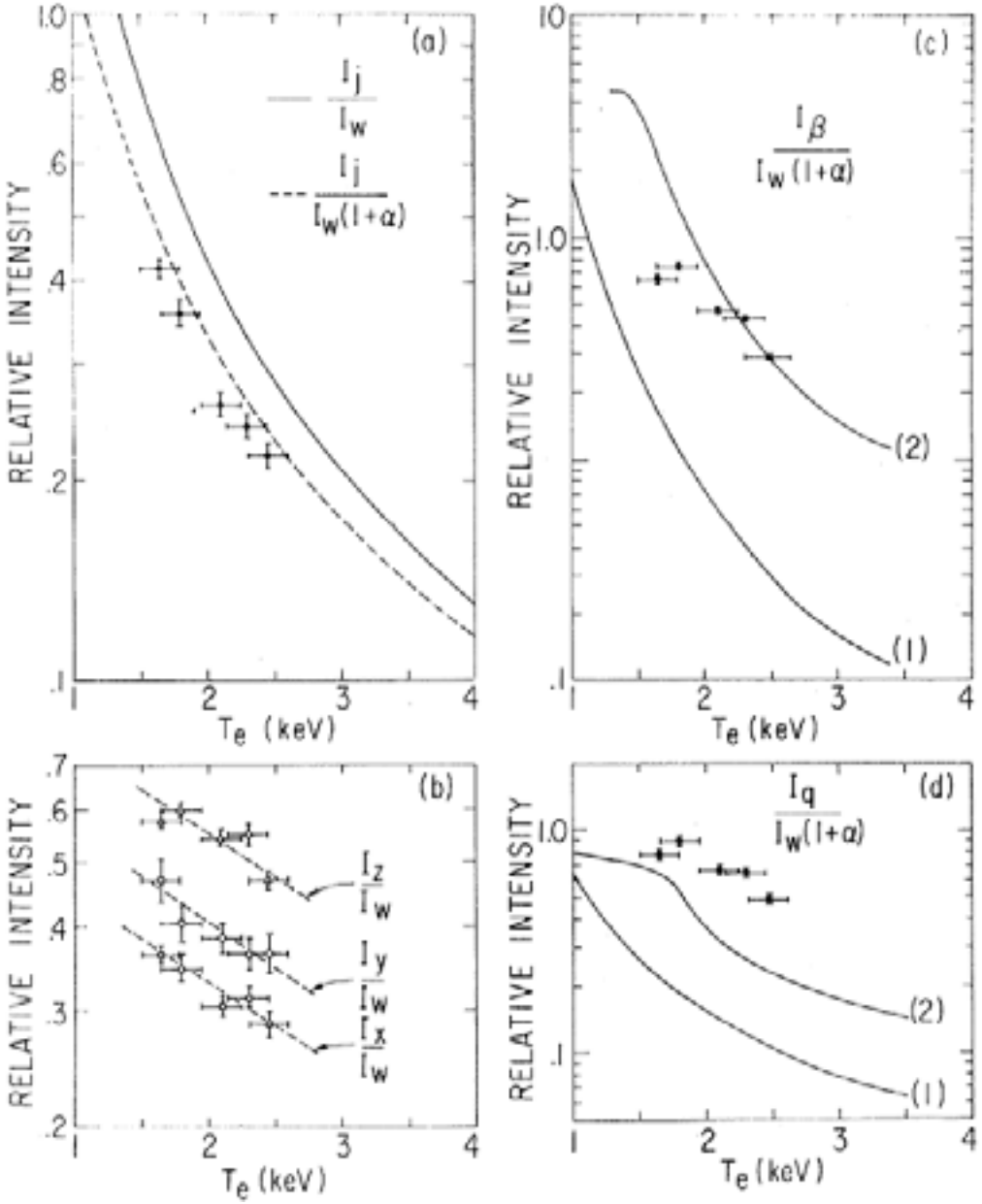

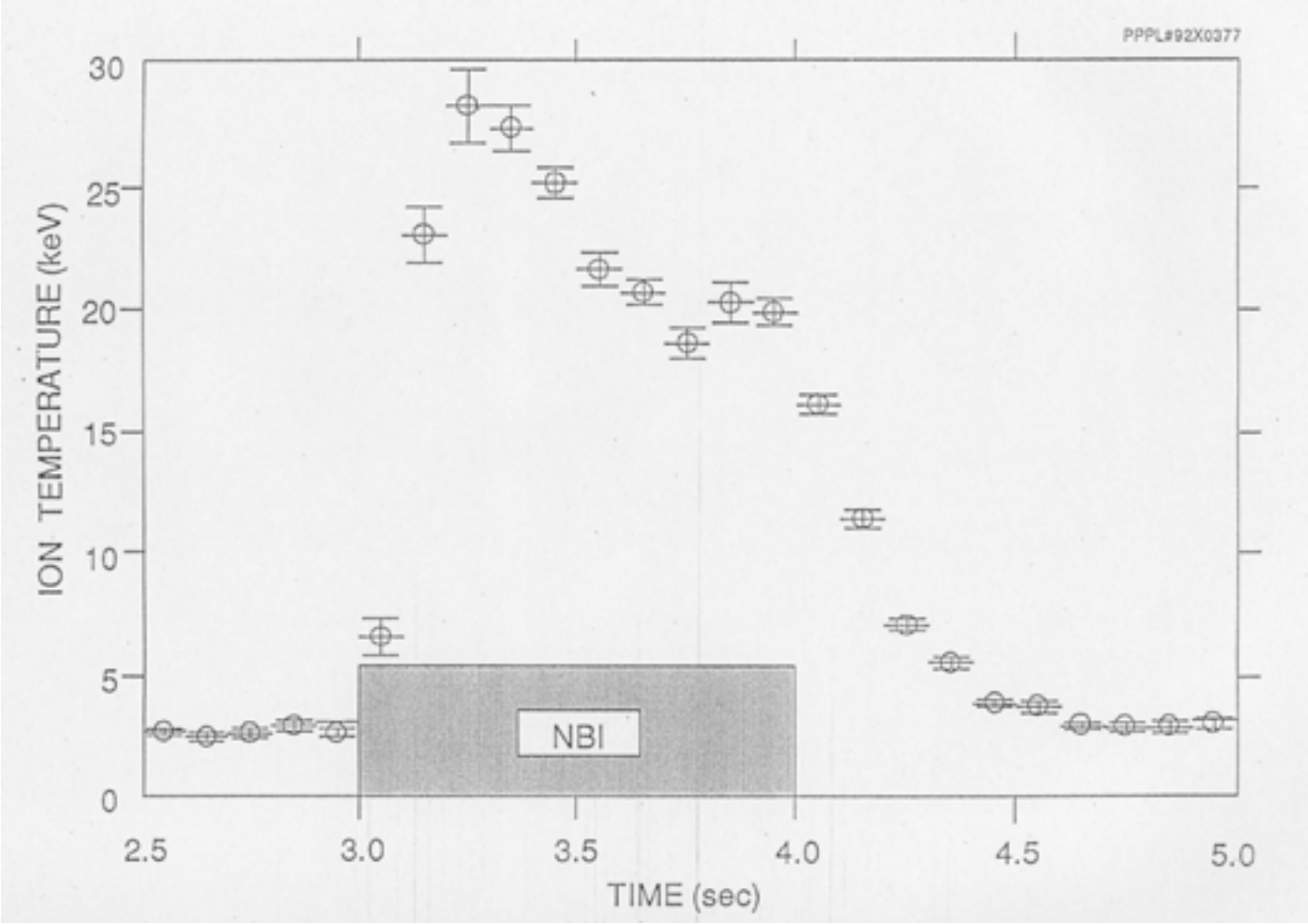
PPPL#92X0377
ION TEMPERATURE (keV)
30
25
20
15
10
5
0
NBI
2.5
3.0
3.5
4.0
4.5
5.0
TIME (sec)

FIG. 7

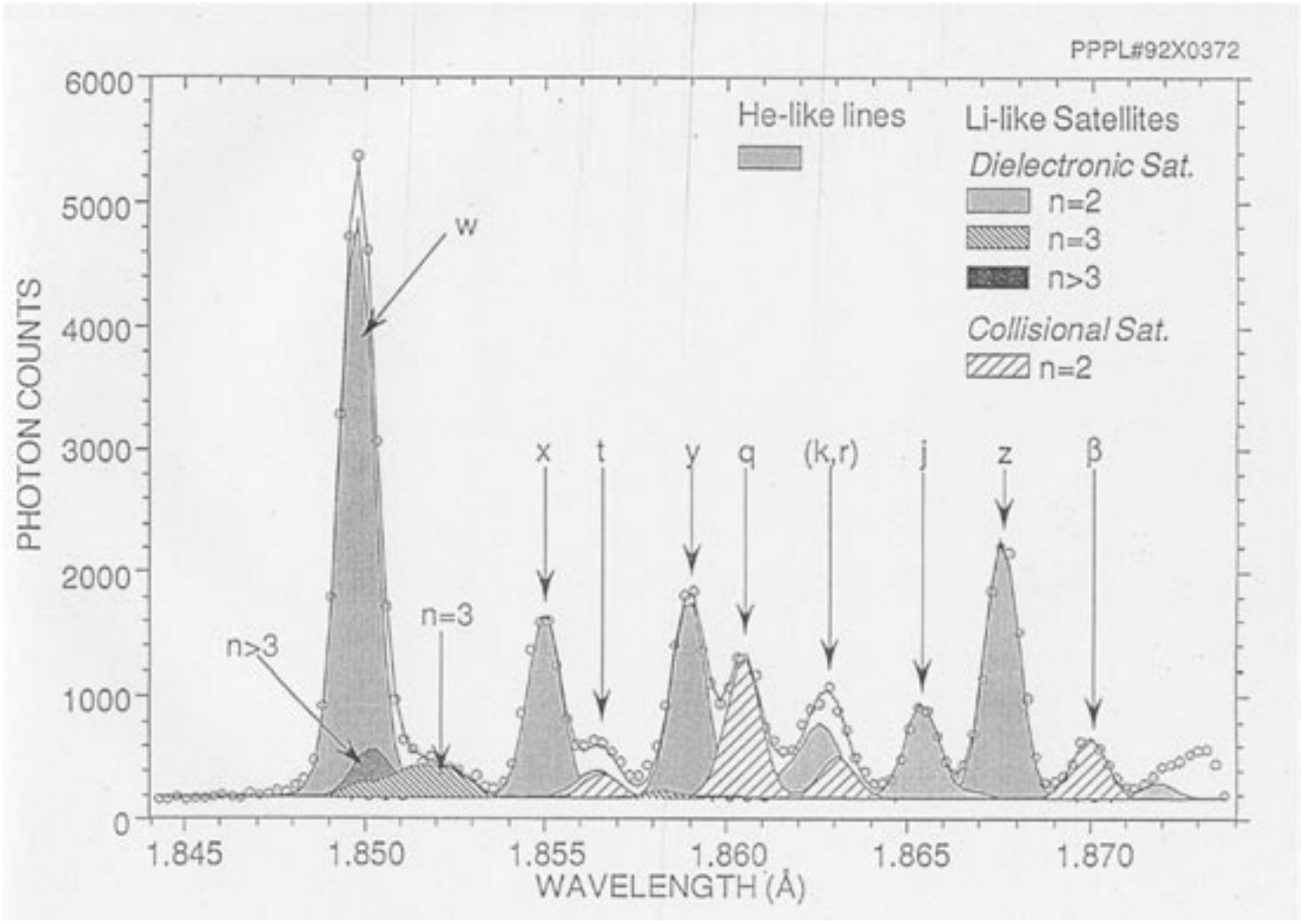
PPPL#92X0372
He-like lines
Li-like Satellites
Dielectronic Sat.
n=2
n=3
n>3
Collisional Sat.
n=2
PHOTON COUNTS
6000
5000
4000
3000
2000
1000
0
w
x
t
y
q
(k,r)
j
z
β
n>3
n=3
1.845
1.850
1.855
1.860
1.865
1.870
WAVELENGTH (Å)

FIG. 8

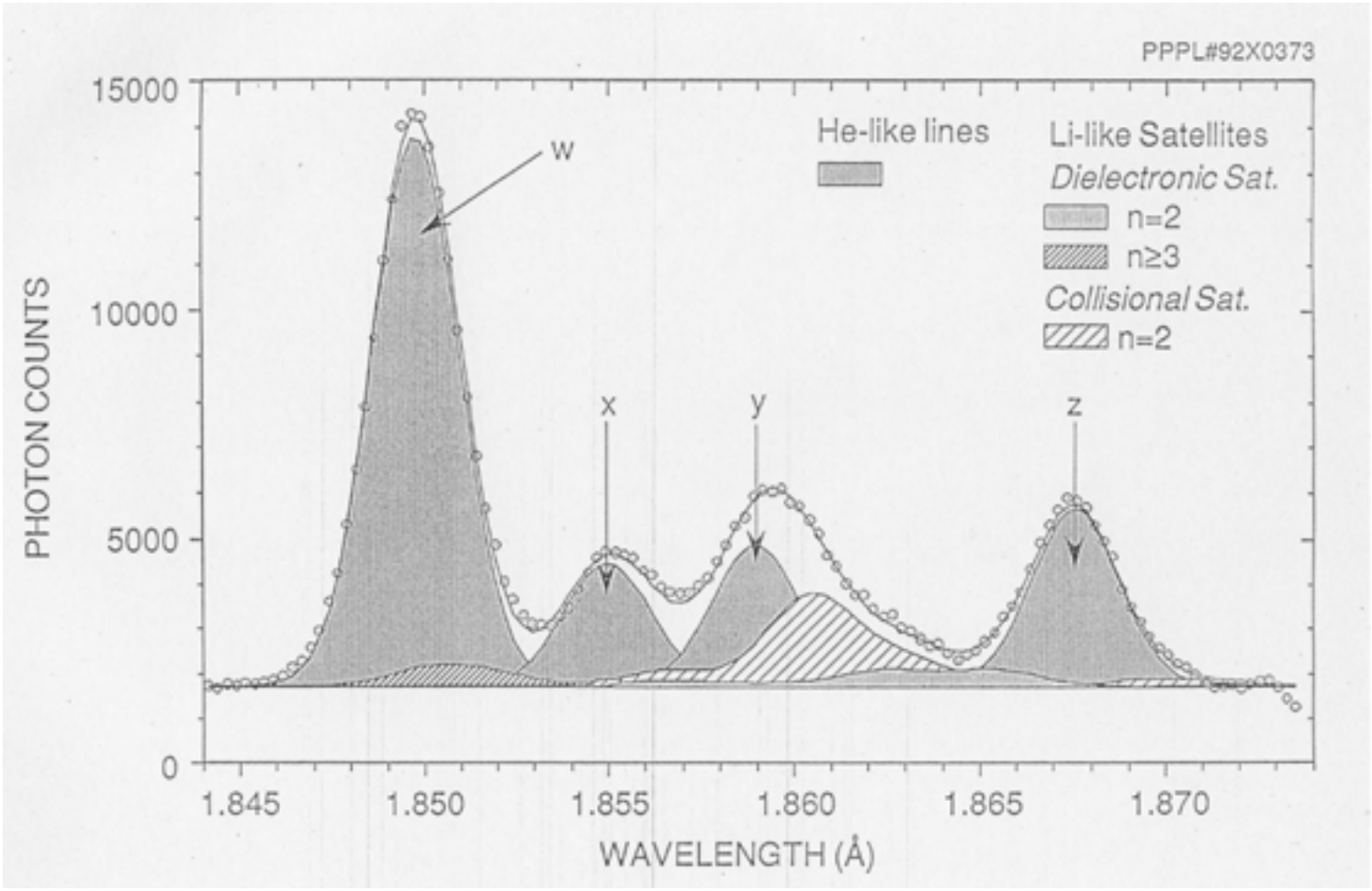
PPPL#92X0373
15000
10000
5000
0
PHOTON COUNTS
w
x
y
z
He-like lines
Li-like Satellites
Dielectronic Sat.
n=2
n≥3
Collisional Sat.
n=2
1.845
1.850
1.855
1.860
1.865
1.870
WAVELENGTH (Å)

FIG. 9

Parameters	Spectrum A	Spectrum B
Ti (keV)	3.2 ± 0.1	20.7 ± 0.3
Te (keV)	3.29± 0.04	8.2 ± 0.04
N_{Li} / N_{He}	0.376± 0.012	0.260± 0.008
N_{Be} / N_{He}	0.144± 0.013	0.018± 0.005
xa *(multiplier)*	1.59± 0.05	2.49± 0.08
ya *(multiplier)*	1.61± 0.04	1.80± 0.04
za *(multiplier)*	1.65± 0.04	2.29± 0.06

FIG. 10

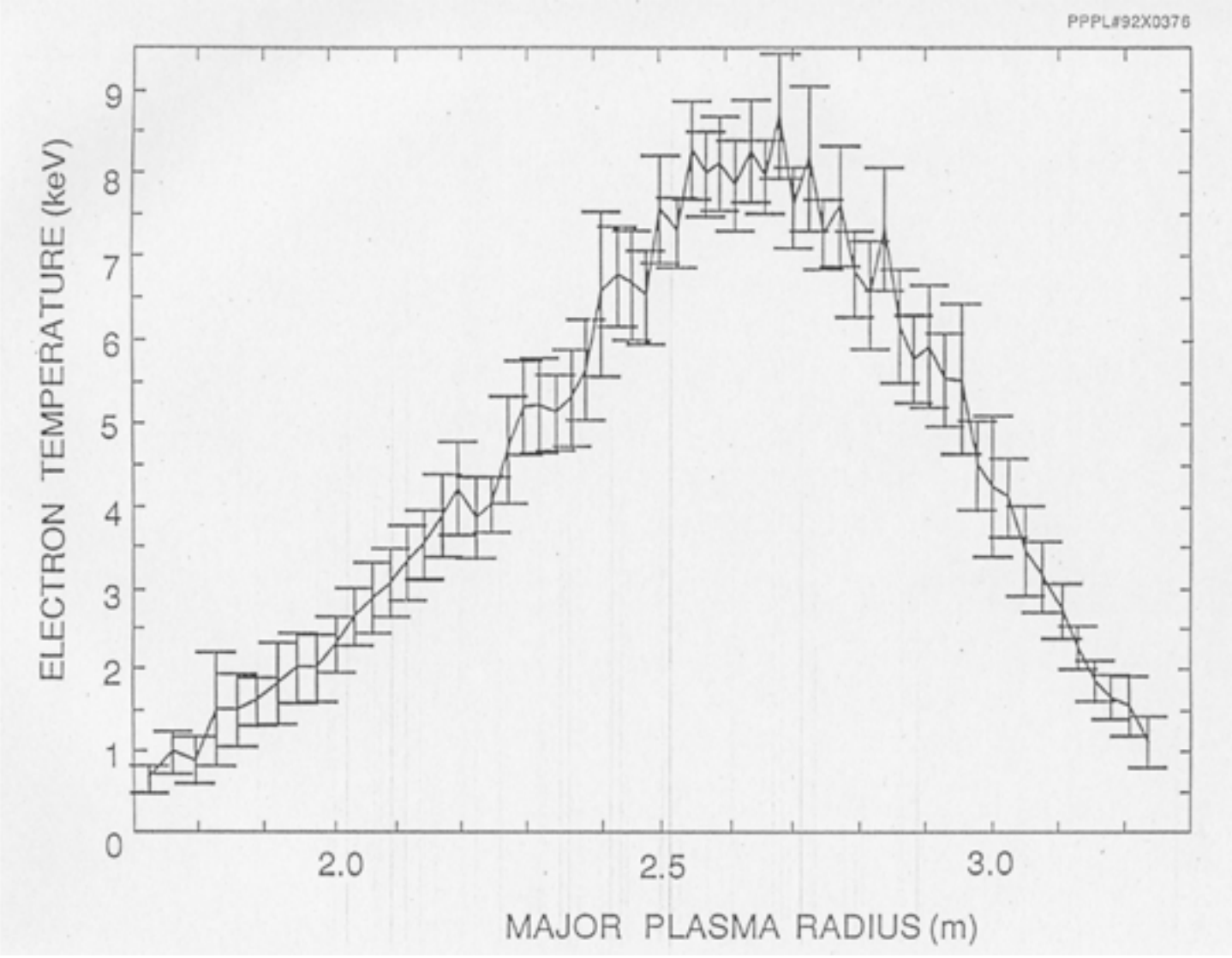
PPPL#92X0376
ELECTRON TEMPERATURE (keV)
0
1
2
3
4
5
6
7
8
9
2.0
2.5
3.0
MAJOR PLASMA RADIUS (m)

FIG. 11

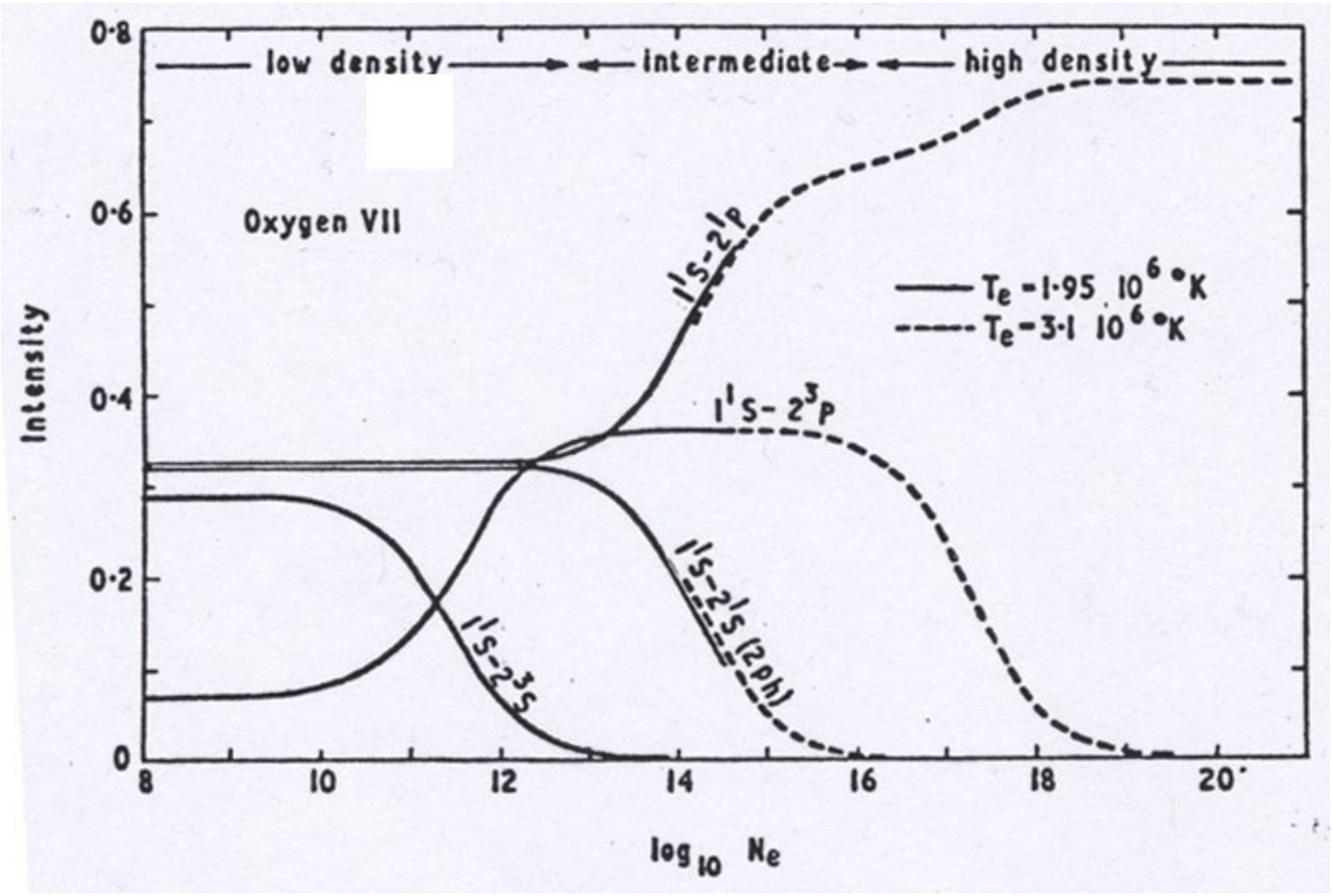
low density
intermediate
high density
Oxygen VII
T_e - 1·95 10^6 °K
T_e - 3·1 10^6 °K
1^1S-2^1P
1^1S-2^3P
1^1S-2^1S (2ph)
1^1S-2^3S
Intensity
0·8
0·6
0·4
0·2
0
8
10
12
14
16
18
20
$\log_{10}$ Ne

FIG. 12

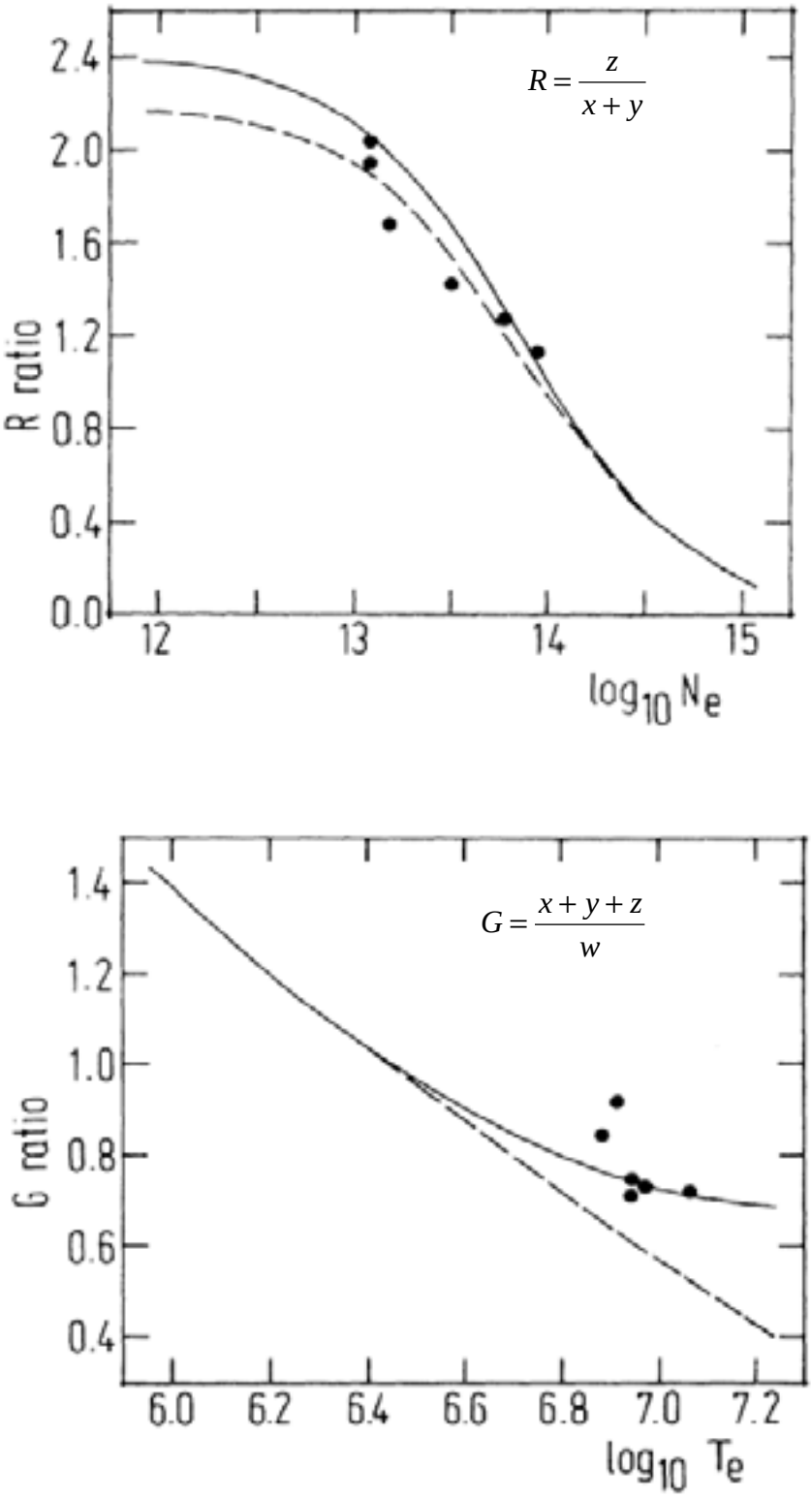
$R = \frac{z}{x+y}$
R ratio
2.4
2.0
1.6
1.2
0.8
0.4
0.0
12
13
14
15
$\log_{10} N_e$
$G = \frac{x+y+z}{w}$
G ratio
1.4
1.2
1.0
0.8
0.6
0.4
6.0
6.2
6.4
6.6
6.8
7.0
7.2
$\log_{10} T_e$

Figure 13

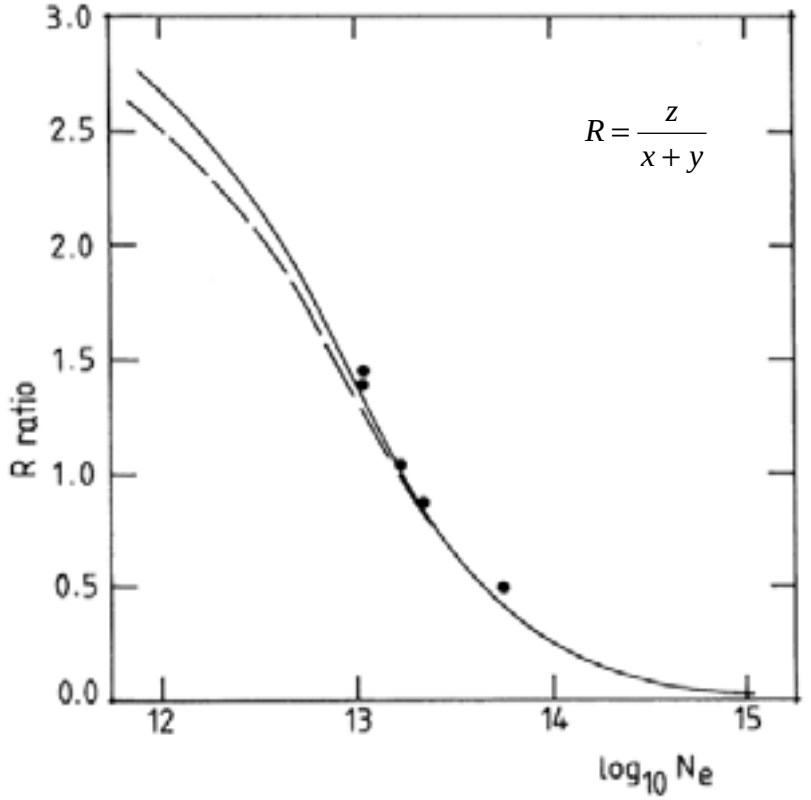
3.0
2.5
2.0
1.5
1.0
0.5
0.0
R ratio
12
13
14
15
log10 Ne
R = z / (x + y)

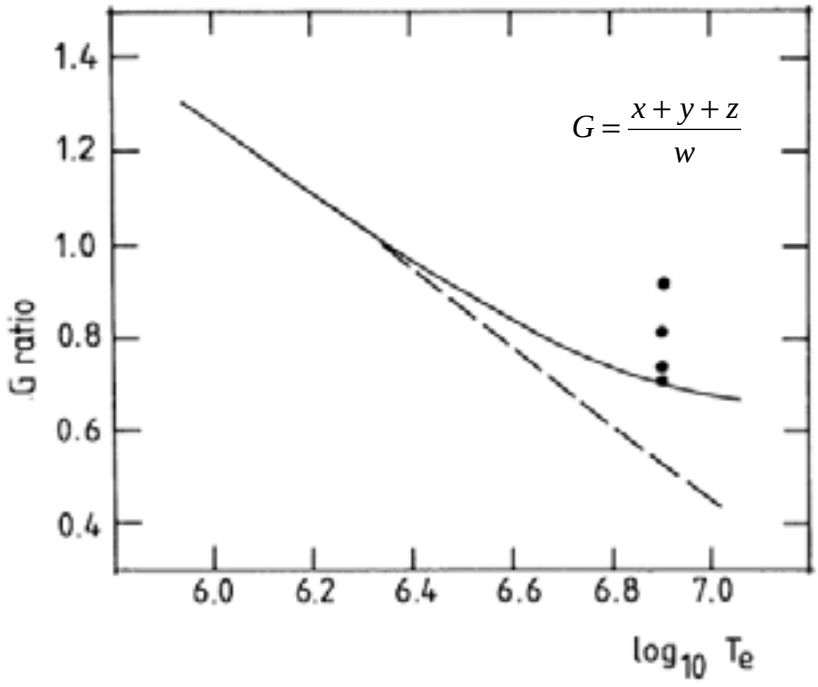
1.4
1.2
1.0
0.8
0.6
0.4
G ratio
6.0
6.2
6.4
6.6
6.8
7.0
log10 Te
G = (x + y + z) / w

Figure 14

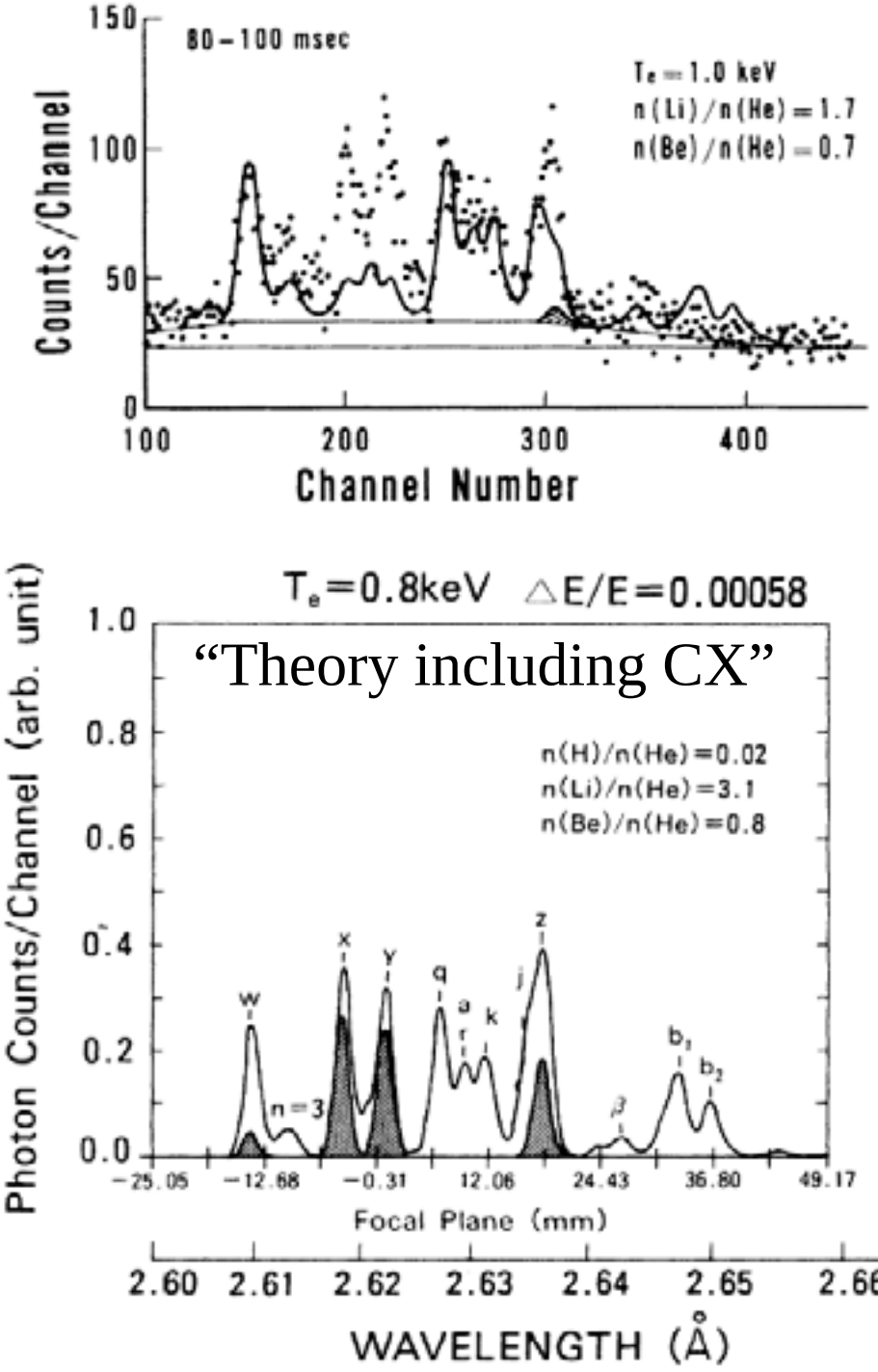
80–100 msec
T_e = 1.0 keV
n(Li)/n(He) = 1.7
n(Be)/n(He) = 0.7
Counts/Channel
Channel Number
T_e=0.8keV △E/E=0.00058
"Theory including CX"
n(H)/n(He)=0.02
n(Li)/n(He)=3.1
n(Be)/n(He)=0.8
Photon Counts/Channel (arb. unit)
Focal Plane (mm)
WAVELENGTH (Å)

Figure 15

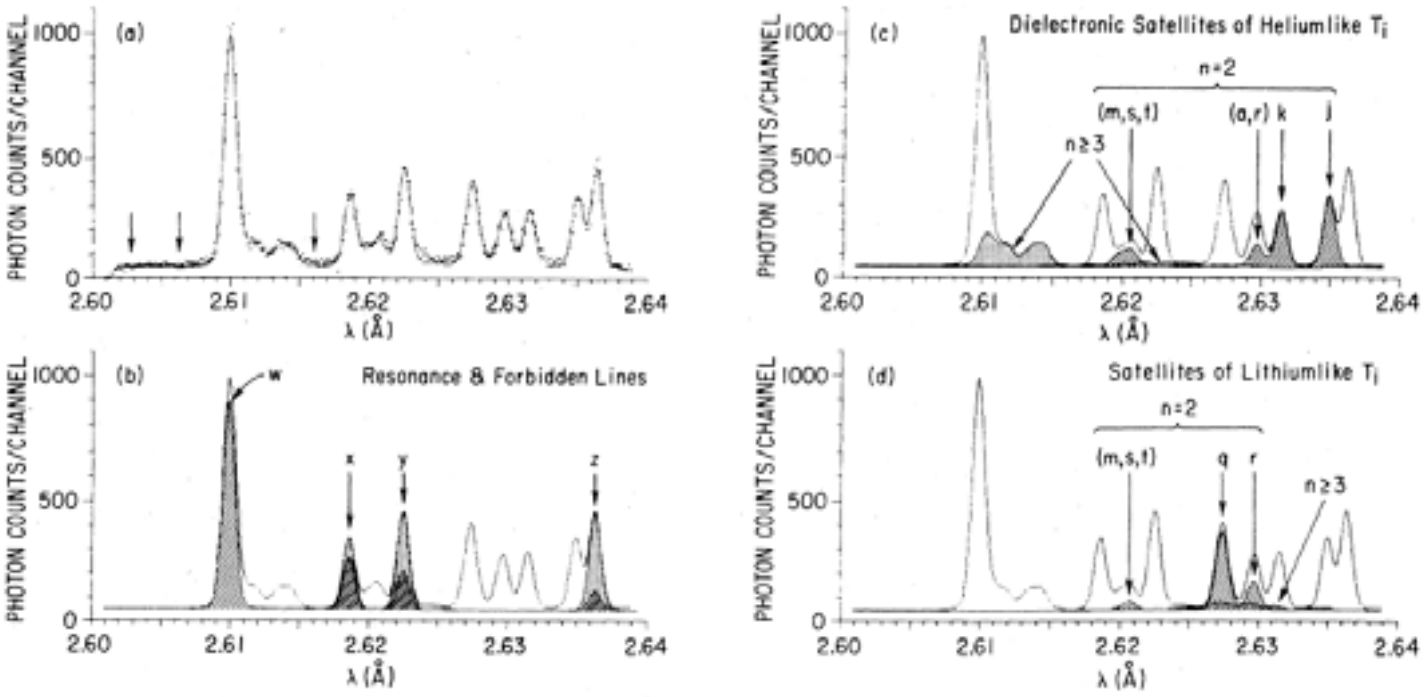
(a)
(b)
Resonance & Forbidden Lines
w
x
y
z
(c)
Dielectronic Satellites of Heliumlike T_i
n=2
(m,s,t)
(a,r)
k
j
n≥3
(d)
Satellites of Lithiumlike T_i
n=2
(m,s,t)
q
r
n≥3
PHOTON COUNTS/CHANNEL
λ (Å)
0
500
1000
2.60
2.61
2.62
2.63
2.64

Fig. 16

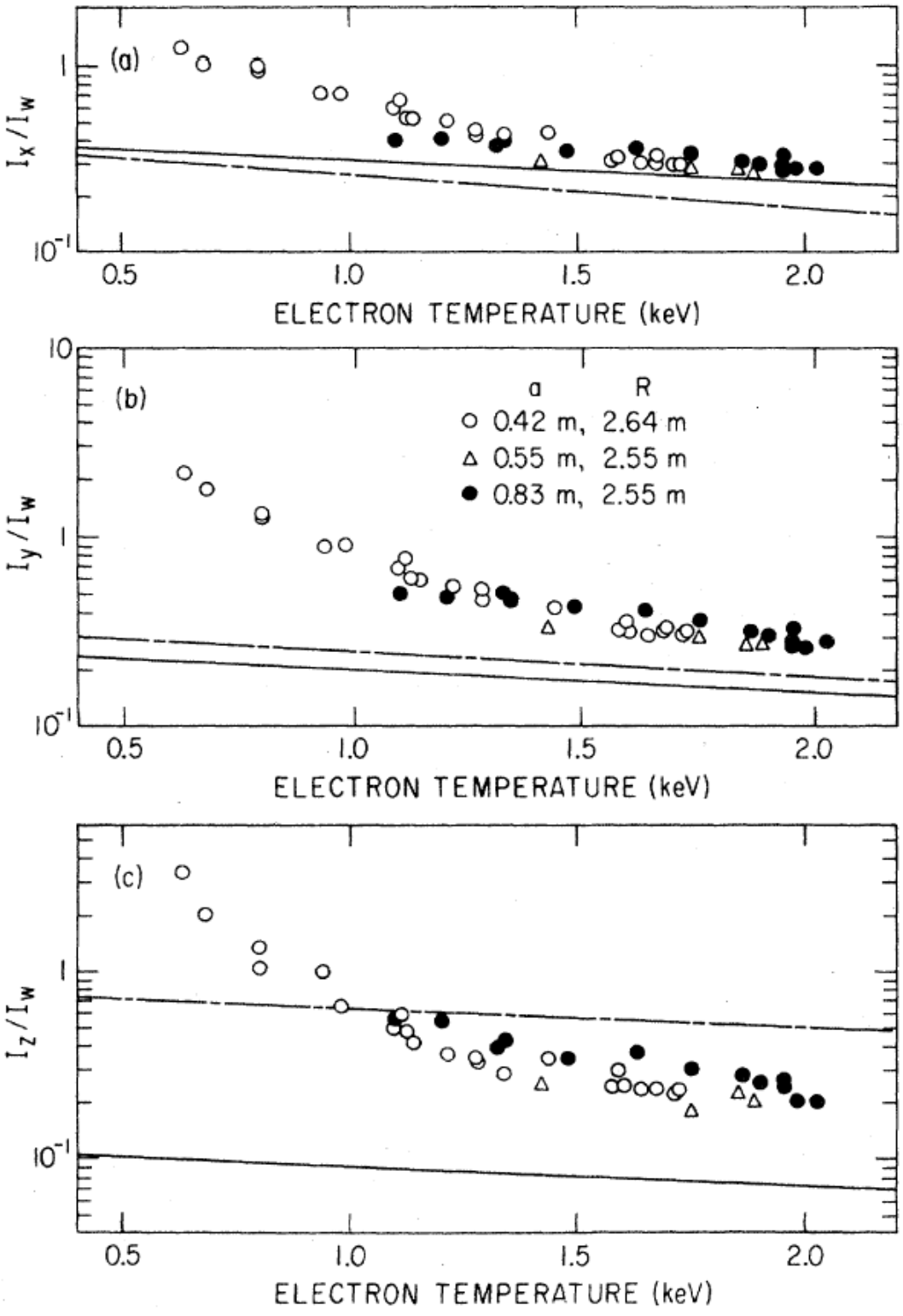
(a)
I_x / I_w
1
10^{-1}
0.5
1.0
1.5
2.0
ELECTRON TEMPERATURE (keV)
(b)
a R
○ 0.42 m, 2.64 m
△ 0.55 m, 2.55 m
● 0.83 m, 2.55 m
I_y / I_w
10
1
10^{-1}
0.5
1.0
1.5
2.0
ELECTRON TEMPERATURE (keV)
(c)
I_z / I_w
1
10^{-1}
0.5
1.0
1.5
2.0
ELECTRON TEMPERATURE (keV)

Fig. 17

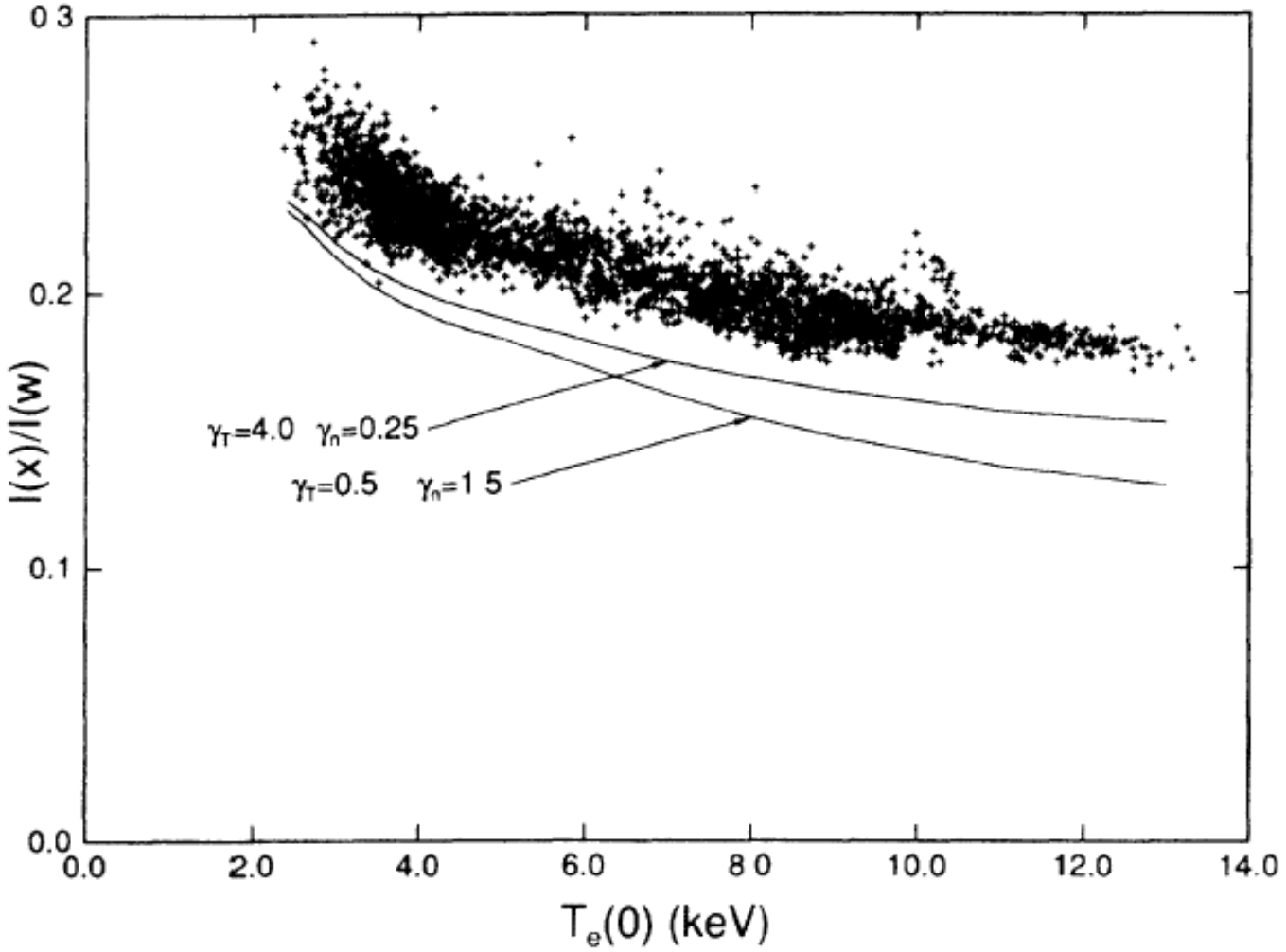
0 3
0.2
0.1
0.0
I(x)/I(w)
γT=4.0 γn=0.25
γT=0.5 γn=1 5
0.0
2.0
4.0
6.0
8 0
10.0
12.0
14.0
Te(0) (keV)

Fig. 18

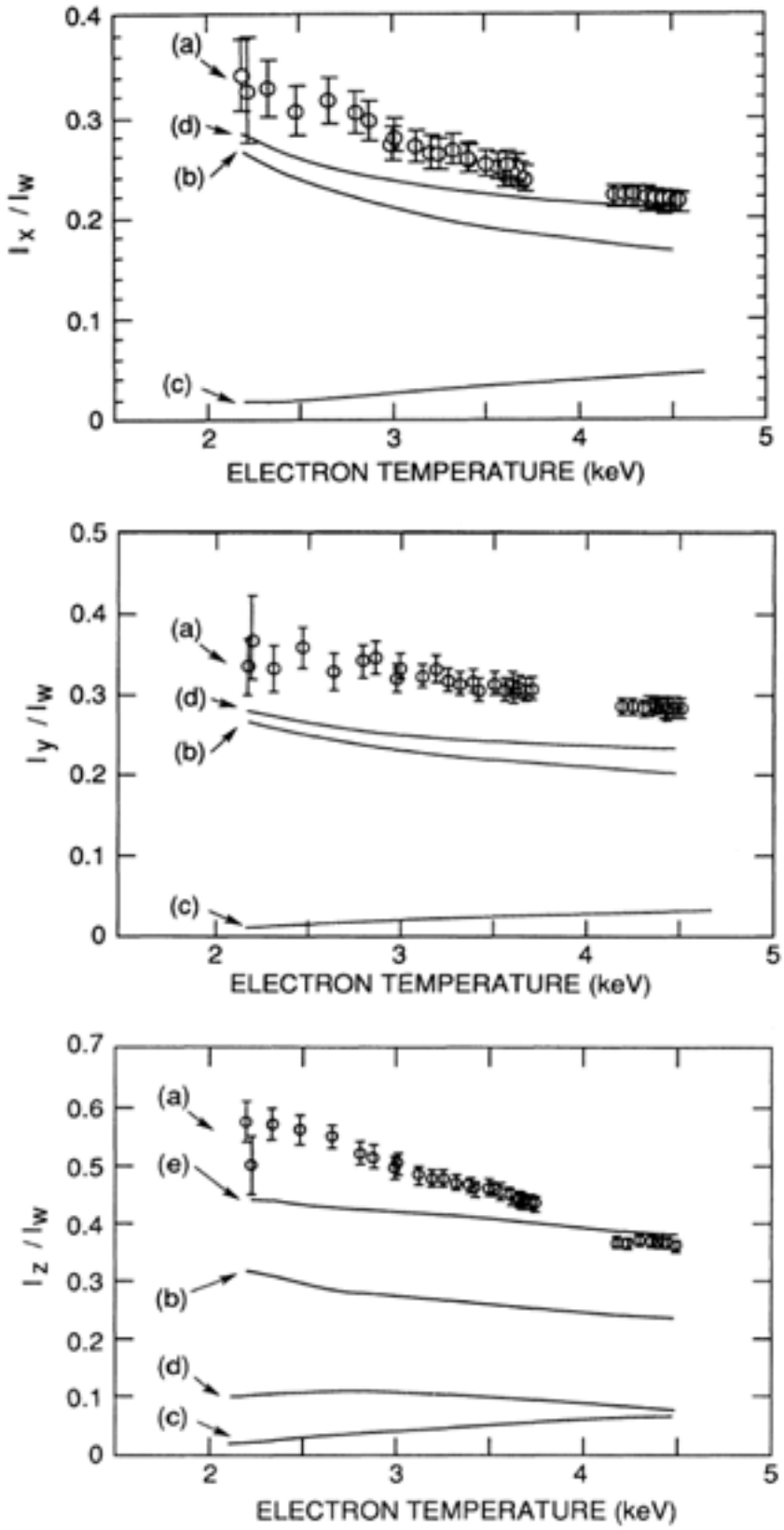
0.4
0.3
0.2
0.1
0
(a)
(d)
(b)
(c)
I_X / I_W
2
3
4
5
ELECTRON TEMPERATURE (keV)
0.5
0.4
0.3
0.2
0.1
0
(a)
(d)
(b)
(c)
I_Y / I_W
2
3
4
5
ELECTRON TEMPERATURE (keV)
0.7
0.6
0.5
0.4
0.3
0.2
0.1
0
(a)
(e)
(b)
(d)
(c)
I_Z / I_W
2
3
4
5
ELECTRON TEMPERATURE (keV)

Fig. 19

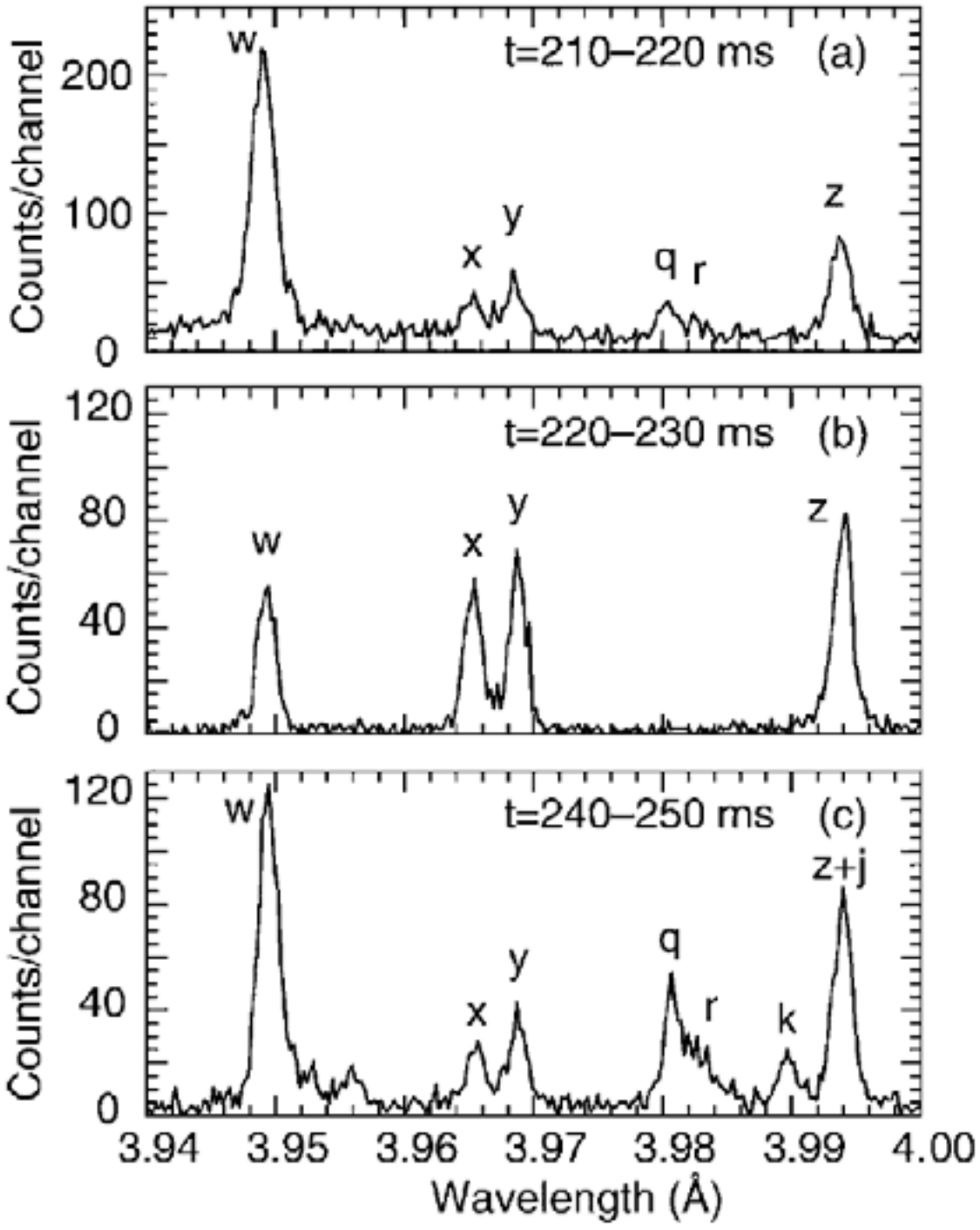
Counts/channel
200
100
0
w
t=210–220 ms
(a)
x
y
q
r
z
120
80
40
0
t=220–230 ms
(b)
w
x
y
z
t=240–250 ms
(c)
z+j
q
r
k
3.94
3.95
3.96
3.97
3.98
3.99
4.00
Wavelength (Å)

Fig. 20

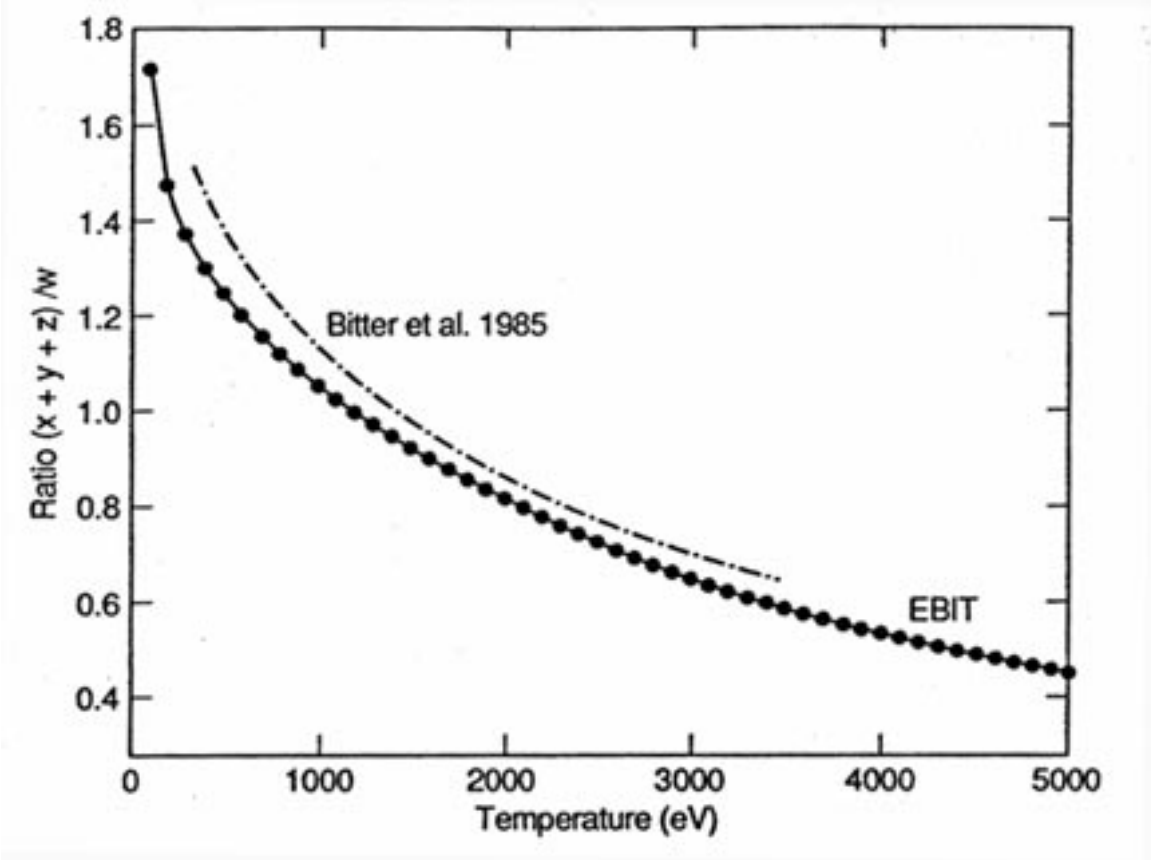
1.8
1.6
1.4
1.2
1.0
0.8
0.6
0.4
Ratio (x + y + z) /w
Bitter et al. 1985
EBIT
0
1000
2000
3000
4000
5000
Temperature (eV)

Fig. 21

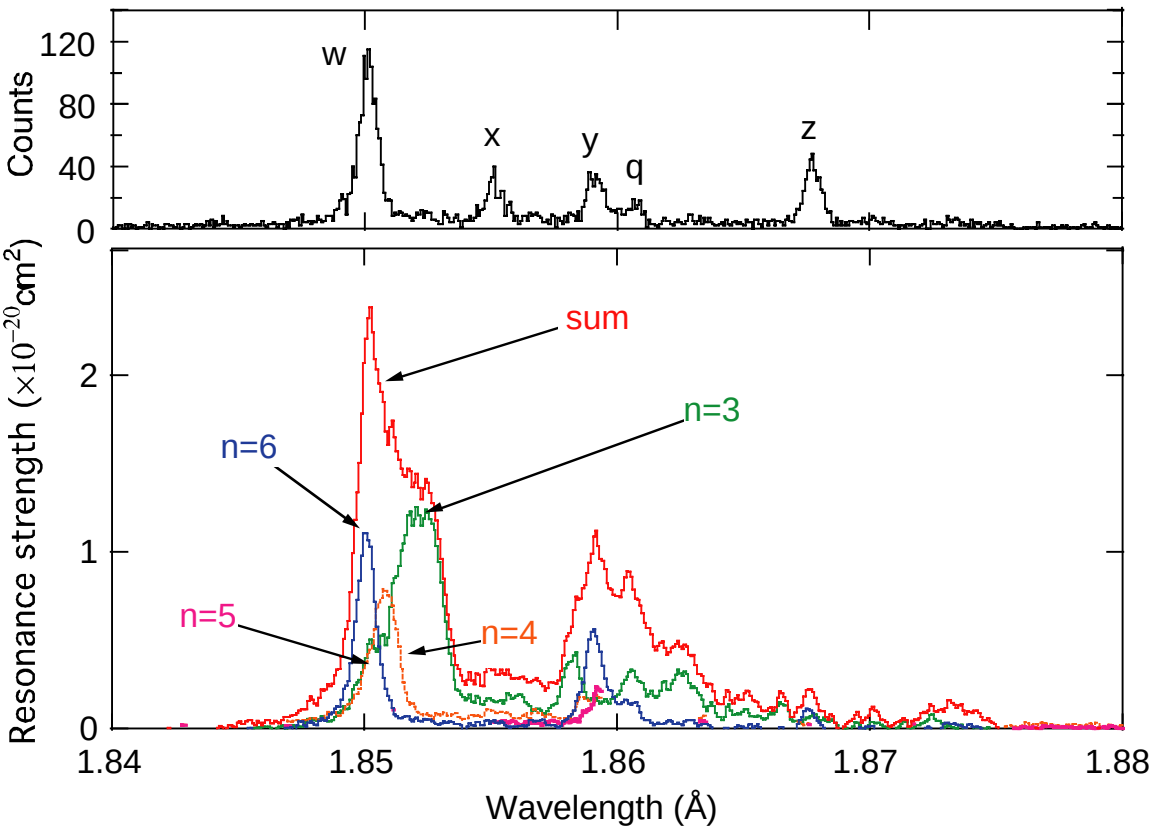
Counts
120
80
40
0
w
x
y
q
z
Resonance strength ($\times 10^{-20}$cm^2)
2
1
0
sum
n=3
n=6
n=5
n=4
1.84
1.85
1.86
1.87
1.88
Wavelength (Å)

Fig. 22

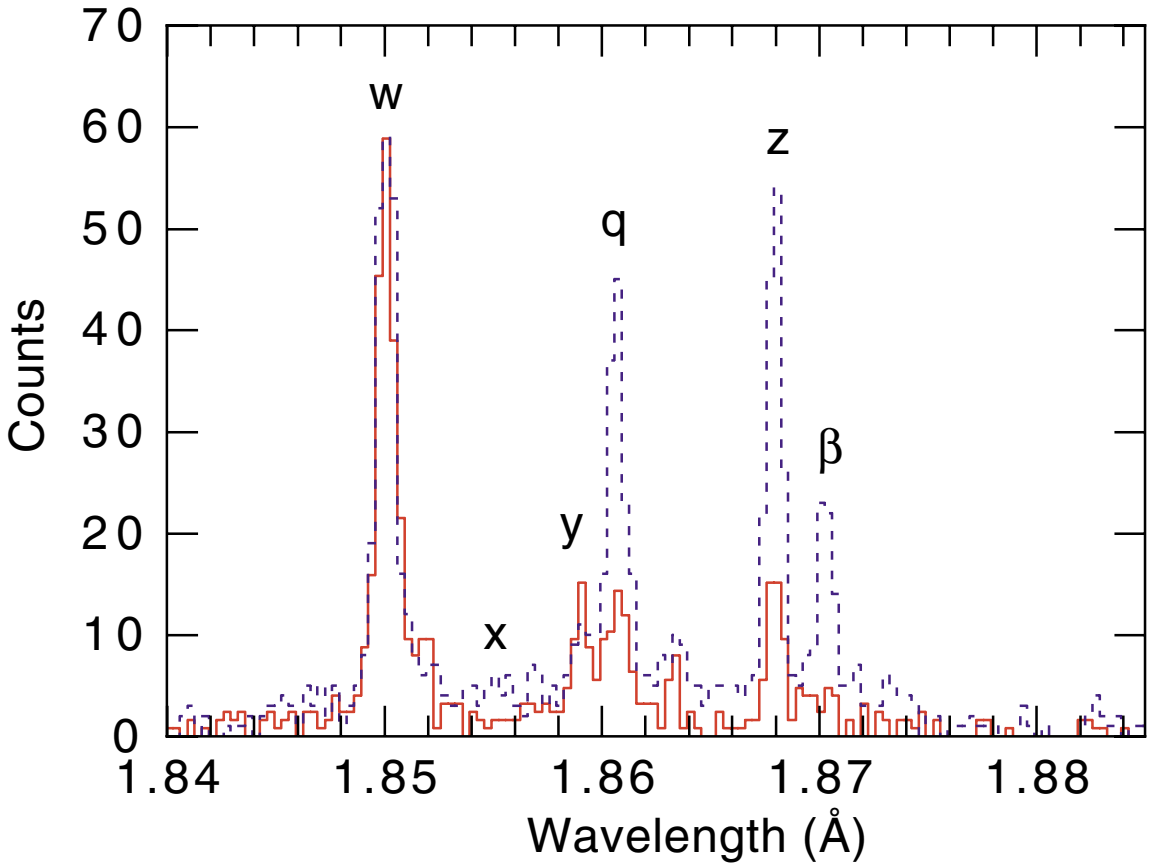
70
60
50
40
30
20
10
0
Counts
w
x
y
q
z
β
1.84
1.85
1.86
1.87
1.88
Wavelength (Å)

Fig. 23

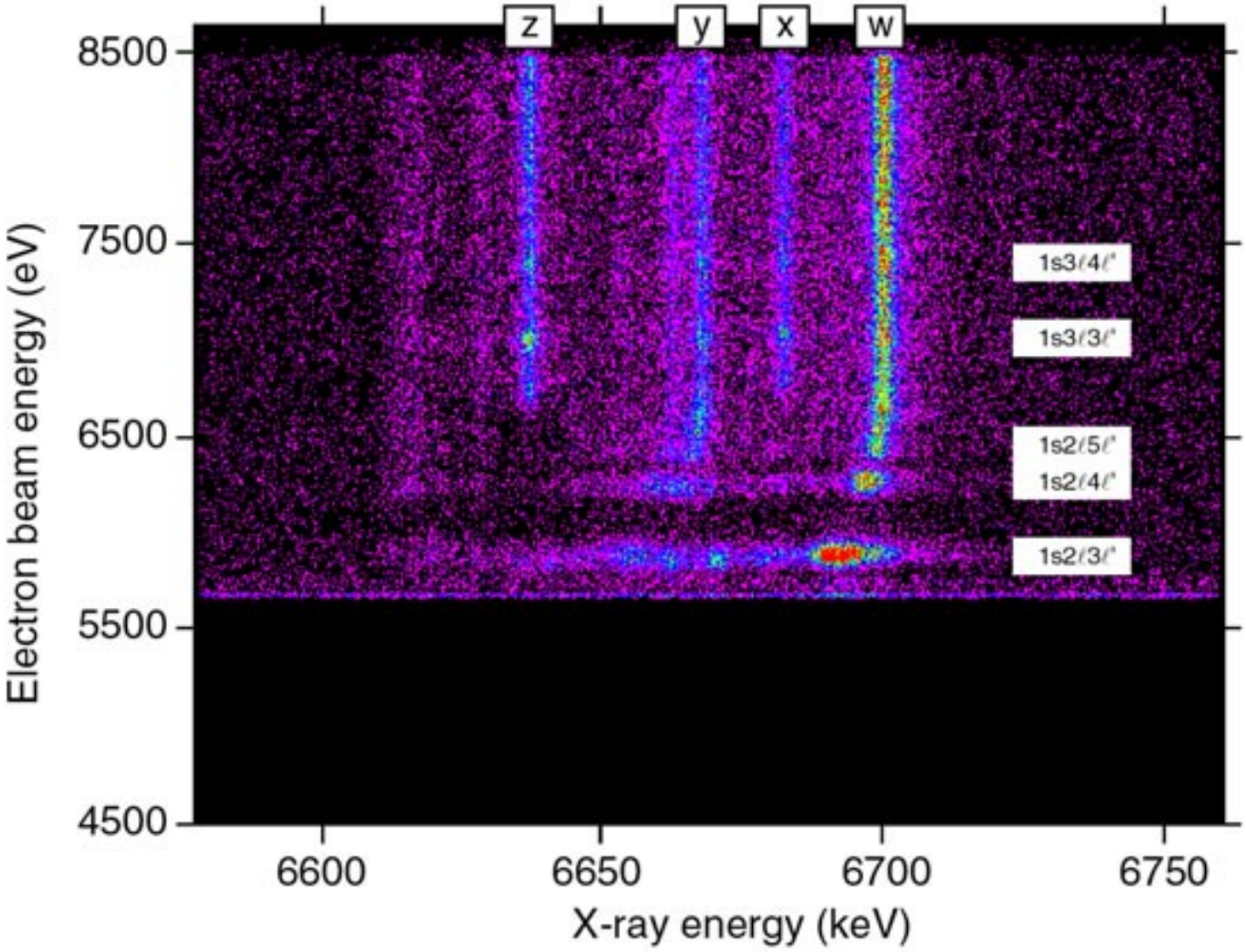
z
y
x
w
8500
7500
6500
5500
4500
Electron beam energy (eV)
1s3/4ℓ'
1s3/3ℓ'
1s2/5ℓ'
1s2/4ℓ'
1s2/3ℓ'
6600
6650
6700
6750
X-ray energy (keV)

Fig. 24

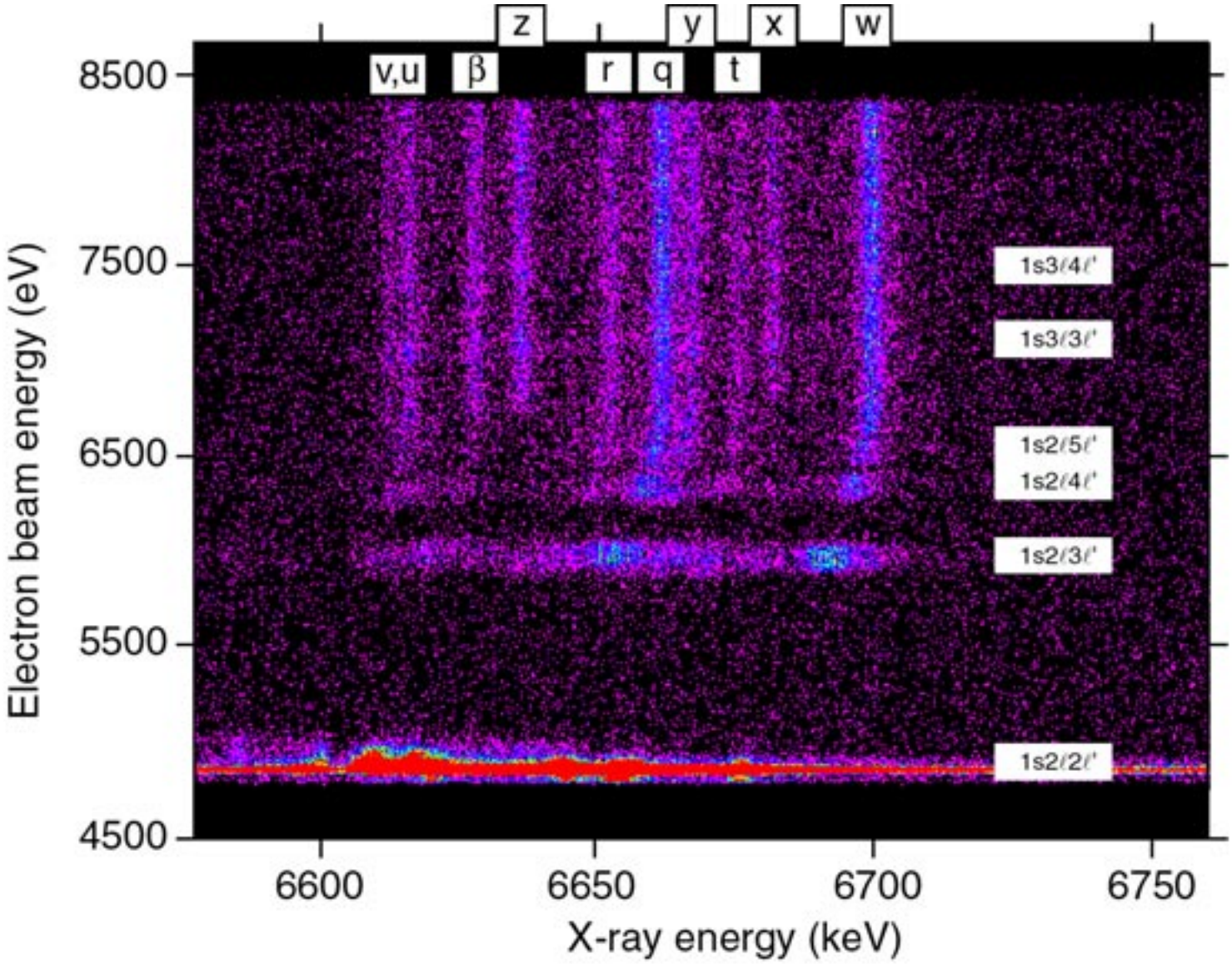
z
y
x
w
v,u
β
r
q
t
8500
7500
6500
5500
4500
1s3/4ℓ'
1s3/3ℓ'
1s2/5ℓ'
1s2/4ℓ'
1s2/3ℓ'
1s2/2ℓ'
Electron beam energy (eV)
6600
6650
6700
6750
X-ray energy (keV)

Fig. 25

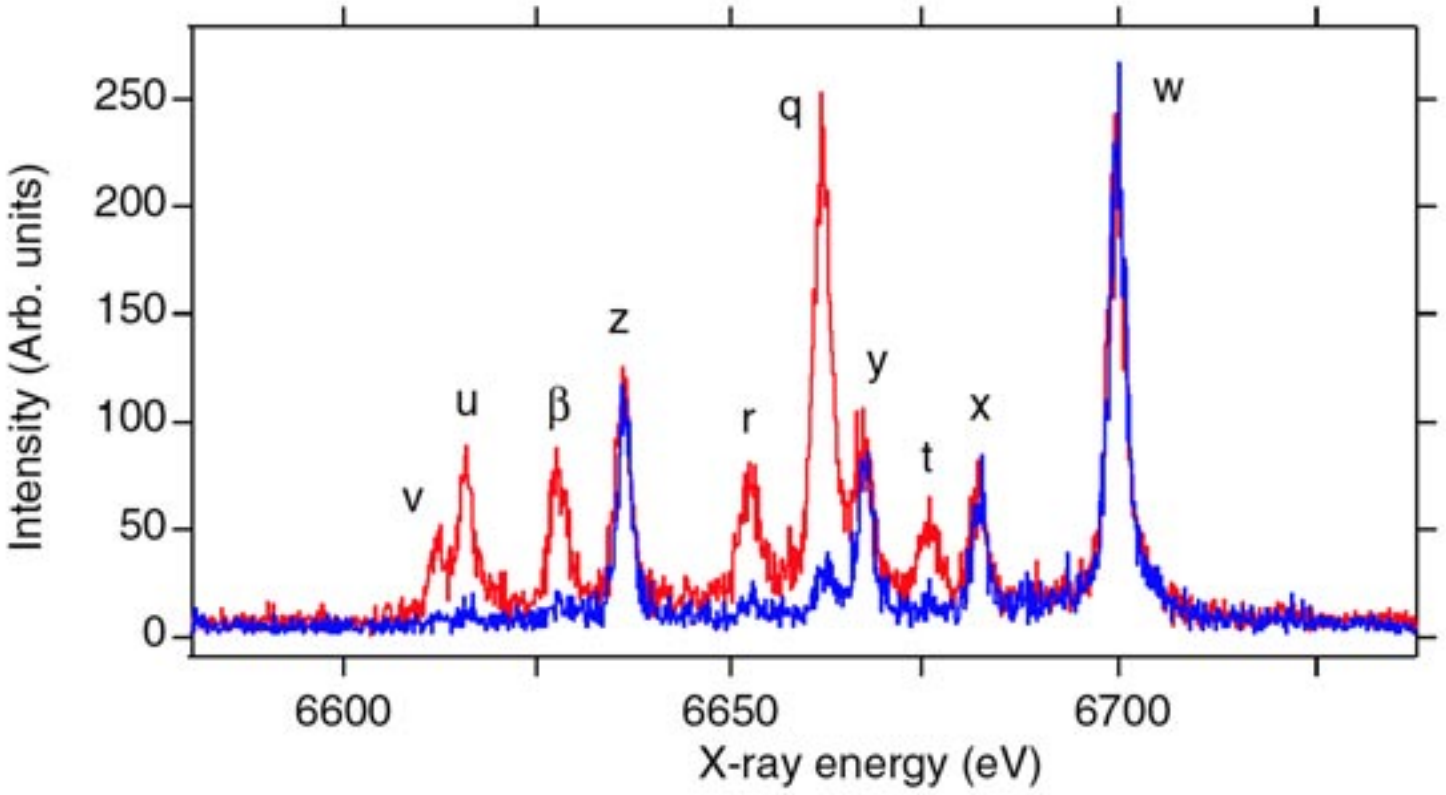
Intensity (Arb. units)
250
200
150
100
50
0
6600
6650
6700
X-ray energy (eV)
v
u
β
z
r
q
y
t
x
w

Fig. 26

Fig 27

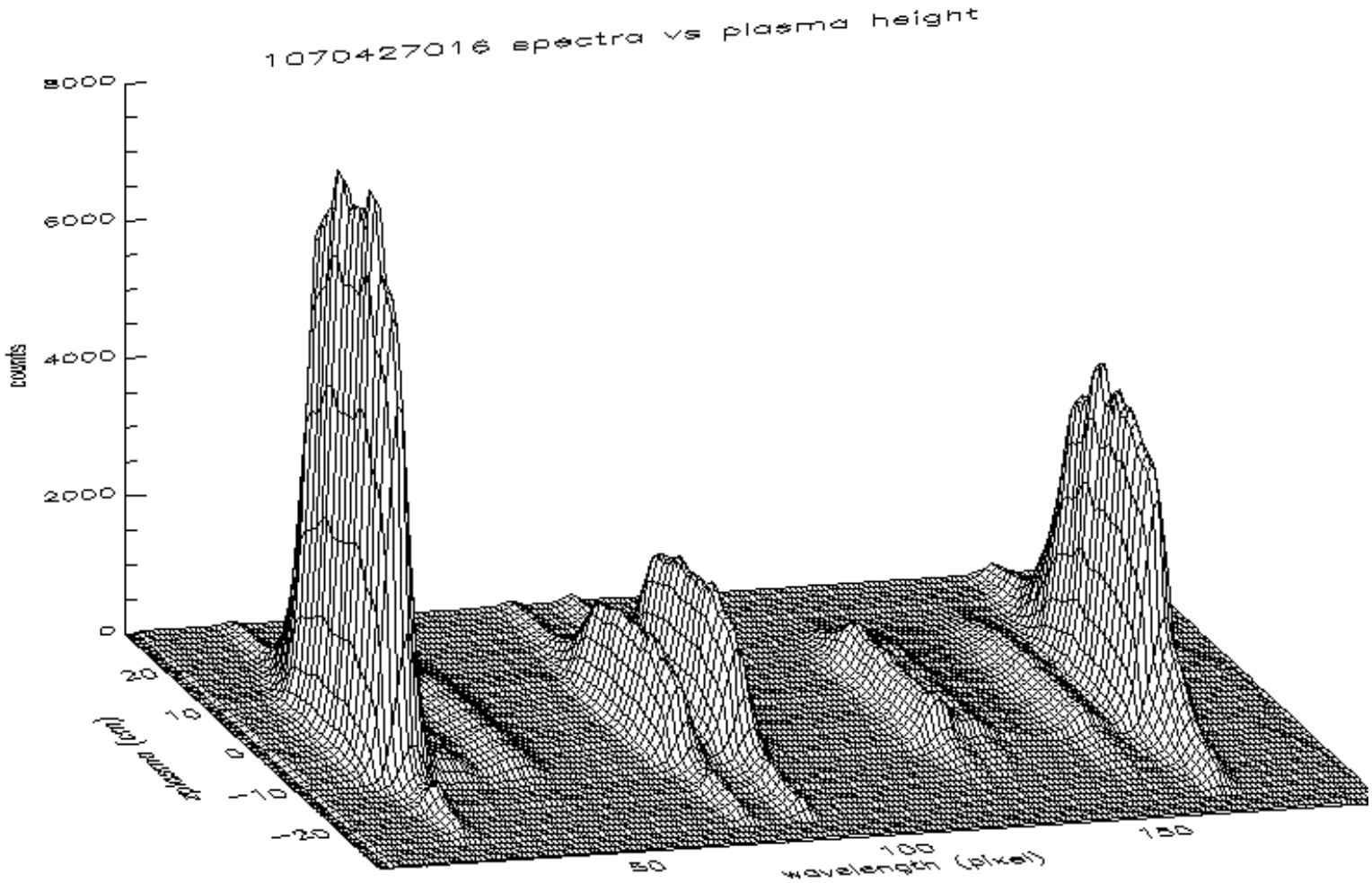
1070427016 spectra vs plasma height
8000
6000
4000
2000
0
counts
20
10
0
-10
-20
(loc) position
50
100
150
wavelength (pixel)